



A 3 million year index for North African humidity/aridity and the implication of potential pan-African Humid periods



Katharine M. Grant ^{a,*}, Eelco J. Rohling ^{a,b}, Thomas Westerhold ^c, Matthias Zabel ^c, David Heslop ^a, Tiuri Konijnendijk ^d, Lucas Lourens ^d

^a Research School of Earth Sciences, The Australian National University, Canberra, Australia

^b Ocean and Earth Science, University of Southampton, National Oceanography Centre, Southampton, UK

^c MARUM, University of Bremen, D-28359 Bremen, Germany

^d Department of Earth Sciences, University of Utrecht, Utrecht 3584 CD, The Netherlands

ARTICLE INFO

Article history:

Received 7 March 2017

Received in revised form

23 June 2017

Accepted 5 July 2017

Keywords:

ODP Site 967

Scanning XRF

Sapropels

African monsoon

Aeolian dust

Plio-Pleistocene

ABSTRACT

Mediterranean sediments are valuable archives of both African monsoon variability and higher-latitude climate processes, and can also be used to provide an environmental context for early human migrations and settlements. However, the long history of Mediterranean palaeoclimate studies largely pre-dates the advent of widespread x-ray fluorescence (XRF) core-scanning, so there are few continuous and high-resolution geochemical records from this key region that extend beyond the last glacial cycle. Here we present XRF core-scanning results for ODP Site 967 (Eastern Mediterranean) that have been fully-calibrated into element concentrations spanning the last 3 million years (My). Comparison with independent geochemical data from conventional XRF highlights disparities for certain element/element ratios, thus suggesting the need for caution when taking ratios of scanning XRF data. Principal component analysis of the calibrated XRF dataset reveals two dominant components: detrital inputs (PC1) and a 'sapropel' (\approx monsoon run-off) signal (PC2), which we use to establish a new orbitally-tuned chronology. We observe inverse covariation between PC2 and a previously published aeolian dust record from ODP Site 967 (Larrasoña et al., 2003), and combine these records to produce a composite index of humidity and aridity for the wider North African region over the past 3 My. We propose that by combining run-off and dust signals in a single metric, our index captures the effects of both strengthening/northward migration (increased run-off) and weakening/southward retreat (increased dust) of the North African monsoon. Comparison of the index with published records of Northwest and East African palaeohumidity suggests that it tracks the timing of "Green Sahara Periods" throughout the Plio-Pleistocene, and that at least 30 of these intervals coincided with increased humidity across East Africa. We tentatively suggest that these specific episodes may be termed "pan-African Humid Periods", as a means to highlight large-scale climate trends and to provide an environmental framework for palaeoanthropological research.

© 2017 Elsevier Ltd. All rights reserved.

1. Introduction

The Eastern Mediterranean is a particularly desirable region for palaeoclimate studies due to its sensitivity to both high- and low-latitude climate processes (Woodward, 2009), and its pivotal location for early human migrations and civilisations. On orbital timescales, strengthening and northward migration of African

monsoon precipitation during boreal summer insolation maxima results in substantially increased freshwater run-off into the Eastern Mediterranean (e.g., Rossignol-Strick et al., 1982; Rohling et al., 2002, 2004; Osborne et al., 2008). Conversely, desertification of the Sahara and Northern Africa when the monsoon rainbelt lies further south causes increased dust deposition in Eastern Mediterranean sediments (Larrasoña et al., 2003). Sea-level changes at these timescales are also registered in the basin (Rohling et al., 2014), due to the sensitivity of Mediterranean $\delta^{18}\text{O}$ to reduced exchange with the Atlantic Ocean (Rohling and Bryden, 1994).

* Corresponding author.

E-mail address: katharine.grant@anu.edu.au (K.M. Grant).

The sensitivity of the basin to African monsoon variability has broader implications, as it provides a well-preserved archive of humid intervals in North Africa, and thus an essential environmental context for archaeological/anthropological research. The most recent of these intervals – the Holocene ‘African Humid Period’ (Ritchie et al., 1985) – is documented by widespread continental evidence in addition to marine proxy records (see Drake et al., 2013; Larrasoña et al., 2013; and references therein); three more “humid” intervals within the last glacial cycle are also fairly well-documented. However, for older intervals, the timing and extent of such ‘Green Sahara periods’ (GSPs) becomes increasingly poorly constrained due to a lack of well-preserved continental deposits with tight chronostratigraphy, and an equal lack of high-resolution marine records. Consequently, the timing of older GSPs is often based on a sequence of organic-rich deposits (‘sapropels’) in the Eastern Mediterranean, which reflect deep-water anoxia and increased primary productivity when monsoon-driven run-off reached the basin (Rossignol-Strick, 1985; Emeis et al., 1996; Rohling et al., 2015). Yet sapropels can be partially or even totally oxidised by post-depositional redox processes (e.g., Higgs et al., 1994; Thomson et al., 1999; De Lange et al., 2008), so the occurrence and/or timing of GSPs based on this approach may be inaccurate if oxidised or ‘ghost’ sapropels are not fully identified. Knowledge of GSPs is crucial for understanding the possible timing and routes of early human migrations and settlements (e.g., Osborne et al., 2008; Drake et al., 2010; Rohling et al., 2013; Timmermann and Friedrich, 2016), especially in conjunction with a growing body of evidence for relatively humid intervals within East Africa over the last few million years (see Maslin et al., 2014).

Given the significance of the palaeoclimate archive contained in Eastern Mediterranean sediments, there is a conspicuous lack of continuous, high-resolution records of bulk element geochemistry from this region that extend beyond the last glacial cycle (~130 ka). For example, geochemical studies of older (>130 ka) Eastern Mediterranean sediments have either focussed on sapropels/limited time intervals (e.g., Passier and De Lange, 1998; Wehausen and Brumsack, 2000; De Lange et al., 2008) or used a relatively low sampling resolution (e.g., Calvert and Fontugne, 2001). Scanning x-ray fluorescence (XRF) records spanning 0–1.7 Ma from the distal Nile Fan were discussed by Zhao (2011), but those records have not been calibrated into element concentrations so the signal may be ambiguous. High-resolution Ti/Al records from ODP Sites 967/968 have been published for the 0–1.4 and 2.2–3.2 Ma intervals (Wehausen and Brumsack, 2000; Lourens et al., 2001; Ziegler et al., 2010; Konijnendijk et al., 2014).

We address this issue by presenting scanning XRF records from ODP Site 967 for the past three million years (3 My) at ~0.3 ky resolution. We use a multivariate log-ratio calibration (Weltje et al., 2015) to convert the scanning XRF data into element concentrations, and then perform a principal component analysis on the calibrated XRF dataset (section 3). We find that the first principal component captures detrital inputs to ODP Site 967, while the second principal component represents a sapropel (hence monsoon run-off) proxy. We use our sapropel/run-off proxy to establish an orbitally-tuned chronology, which we evaluate against previous chronologies for this site (section 4). Finally, we present a new index of humidity/aridity for the wider northeastern Saharan/North African region over the past 3 My, based on our sapropel/run-off proxy and a previously published (Larrasoña et al., 2003) aeolian dust record from the same site.

2. Methods

ODP Site 967 (34° N, 34°E, 2252 m water depth; hereafter, ‘ODP967’) is situated on the Eratosthenes seamount and was drilled

during ODP Leg 160 (Emeis et al., 1996) (Fig. 1). A new composite depth splice was established (Supplementary Table 1) so that our chronostratigraphy could be based as much as possible on the sampled core sections. This ensured that depth/age uncertainties associated with adjusting ‘off splice’ samples to the composite splice were minimised. Konijnendijk et al. (2014) also published a composite-depth splice for ODP967. However, that splice is partly based on ODP Site 968, and it doesn’t cover the lower 45 m of our studied interval. All previous results from ODP967 discussed in this study have been converted to our new composite depth scale.

2.1. X-ray fluorescence (XRF)

Approximately 90 m of the archive halves of ODP Site 967 cores were scanned at 1 cm intervals at Marum – Center for Marine Environmental Sciences, University of Bremen (Germany) on a third generation Avaatech XRF core scanner. Core sections were covered with 4 µm-thick Ultralene film and measured at 50 kv with a 1 mA current and Cu filter, and then at 10 kv with a 0.5 mA current and no filter; a 20 s count time was used for both runs. To convert the scan ‘counts’ into element concentrations, 40 bulk sediment samples of ~2 cm³ were taken from selected working halves equivalent to the scanned archive halves. Samples were chosen to cover a range of lithologies (e.g., sapropel, clay, sapropel-clay intergrades) based on the XRF scan results, as well as a range of depth intervals. The samples were air-dried and ground with an agate mortar and pestle. Single element concentrations were determined on the sediment powder samples by energy-dispersive polarisation XRF (EDP-XRF) spectroscopy using a PANalytical epsilon3-XL instrument at the University of Bremen. High quality control of the EDP-XRF measurements was based on more than 60 certified and in-house standard reference materials (e.g., MAG-1; Govindaraju, 1994). The measured values were within 1% of the accepted value for Al, Ca, Fe and K. Precision was always better than 0.4%.

2.2. Calibration of scanning XRF counts

Uncertainties in the output scanning XRF counts can be reduced by calibrating the scan data with a representative suite of discrete sub-samples from the same core, which have been analysed using a more quantitative geochemical technique. Calibration is also necessary if multivariate statistical analyses are to be performed on the scanner data. Element counts from the XRF scans were therefore converted into concentrations using a multivariate log-ratio calibration (MLC), following Weltje et al. (2015). This approach builds on the previously proposed univariate log-ratio calibration (Weltje and Tjallingii, 2008), but instead calibrates all elements simultaneously using centred log-ratios, thereby enabling elements that were not adequately captured by the scanning XRF (typically those with an atomic mass less than that of Al) to be taken into account in the calibration. This undefined variable is here termed ‘everything else’, hence the relative concentrations of all scanned elements and ‘everything else’ sums to 100%.

The predictive power of our calibration can be assessed by cross-plotting the reference concentrations with the MLC results (Supplementary Fig. 1). High r^2 values for all elements indicate a robust calibration, which is strongest for Ca and Sr ($r^2 = 0.93$) and weakest for Zr ($r^2 = 0.68$). Nonetheless, when considering the predicted concentrations over all depths, the calibration infers some anomalously high concentrations for Ba (>10,000 ppm) compared to results from conventional XRF analyses of ODP967 (<2000 ppm; this study and that of Konijnendijk et al., 2014). As the data are compositional, outliers in the calibrated XRF dataset were detected using the Mahalanobis distance (Rousseeuw and van Zomeren, 1990), which is specifically designed for

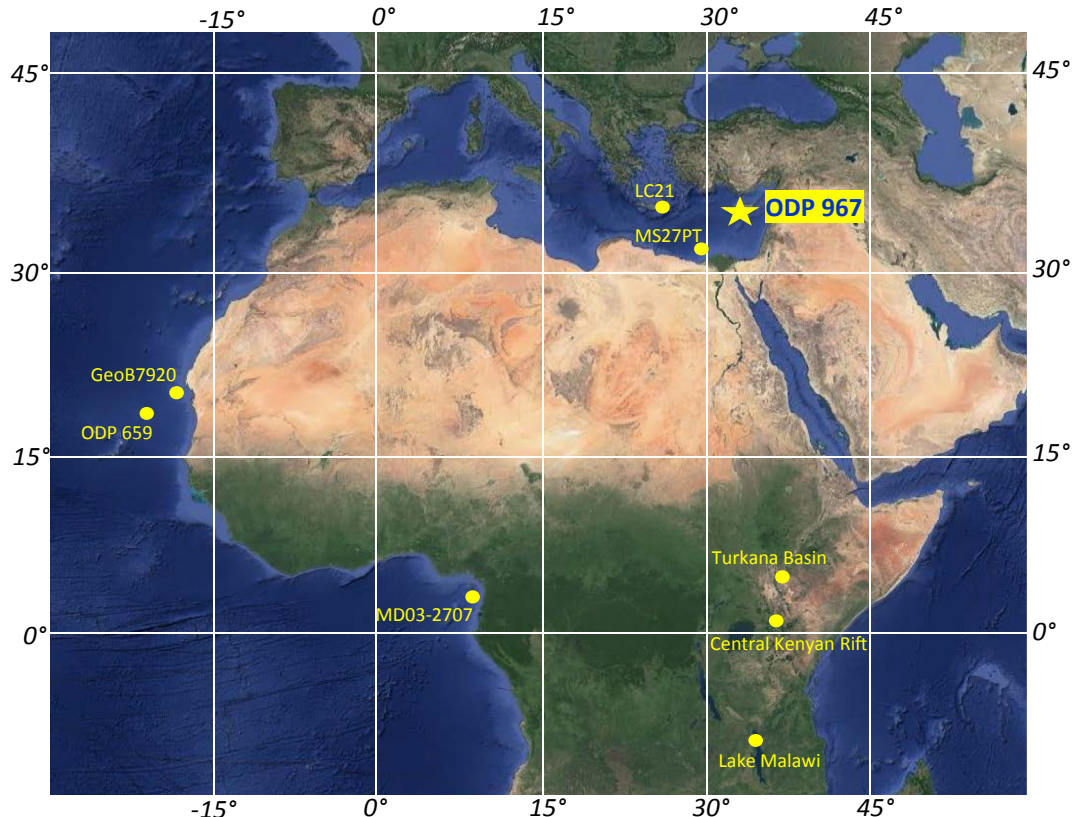


Fig. 1. Location map of cores discussed in this study.

multidimensional data and accounts for correlations within the dataset (as is the case with sediment geochemical compositions). The Mahalanobis distance, d , for the i th depth is given by:

$$d_i = \sqrt{(x_i - T(X)) \cdot C(X)^{-1} \cdot (x_i - T(X))^t} \quad (1)$$

where x_i corresponds to the composition of the i th sample, $T(X)$ is the mean composition of the dataset X , $C(X)$ is the dataset covariance matrix and t corresponds to the matrix transpose. Using the interquartile range (IQR) to detect outliers, “mild” outliers are typically considered to be beyond the 3rd quartile + 1.5*IQR, and “extreme” outliers are beyond the 3rd quartile + 3*IQR. However, using these cut-offs does not remove all obvious Ba outliers (Supplementary Fig. 2). We therefore empirically determined a cut-off value for d , based on the calibrated Ba data, which appeared to remove all outliers and still maintain the integrity of the dataset (10% of the data was removed) (Supplementary Figs. 2 and 3). The depths of all outliers are associated with sapropels, and coincide with lows in ‘everything else’. Sapropels are rich in organic matter and may be poorly retained within opened sediment cores due to their crumbly texture. This was the case with several sapropels in the scanned core sections, which were opened over 15 years ago. XRF core-scanners cannot measure organic carbon, and record lower counts for porous/crumbly sediments. The calibration problem at a few points within some sapropels is therefore most likely due to compromised (too low) scan counts.

3. Results

3.1. XRF calibration

The calibrated concentrations generally show excellent

agreement with previous conventional XRF analyses of ODP967 (Konijnendijk et al., 2014; hereafter, ‘TK2014’) (Fig. 2). The comprehensive TK2014 dataset is especially useful for validating our calibrated scanning XRF data because it spans ~20 m of composite depth at mostly 2 cm resolution, and is independent of our calibration. The TK2014 splice also includes core sections from ODP Site 968, so only the ODP967 component of TK2014 (adjusted to our new composite depth scale) is considered here. Given the widely documented sources of uncertainty in scanning XRF analyses (see Rothwell and Croudace, 2015; and section 5.1), the near-identical results from our study and TK2014, for all elements except K (Fig. 2), are impressive, and unequivocally validate our results. For Si and Al, trends are similar but off-set.

We also evaluate our calibrated XRF results in terms of element ratios, since these are frequently the basis of palaeoclimatic interpretations from scanning XRF data. Prior to taking ratios, all records were smoothed using a 5 cm Gaussian window. Element/Al and element/Ca ratios were then examined since both have been proposed as useful indices in marine sediment studies (e.g., Rothwell and Croudace, 2015; Hennekam and De Lange, 2012) and at ODP967 in particular (Wehausen and Brumsack, 2000). Comparing first our element/Al ratios with those of TK2014 (Fig. 3), we see an excellent agreement for Ca/Al, Sr/Al, Mn/Al and Ba/Al, generally good agreement for Fe/Al, and varying degrees of offset for Si/Al, K/Al, Zr/Al and Ti/Al. Our K/Al record in particular shows no resemblance to that of TK2014, while our Ti/Al and Zr/Al records match the equivalent TK2014 records in places but not consistently. The Si/Al records agree better if a 0.5 offset is applied. In contrast, excellent agreement is observed between the TK2014 records and ours for almost all element/Ca ratios, and to a lesser extent for Sr/Ca (Fig. 4). The Sr/Ca ratio shows the lowest values (order of 10^{-3}), so the signal-to-noise ratio is extremely low. In that case, some offsets

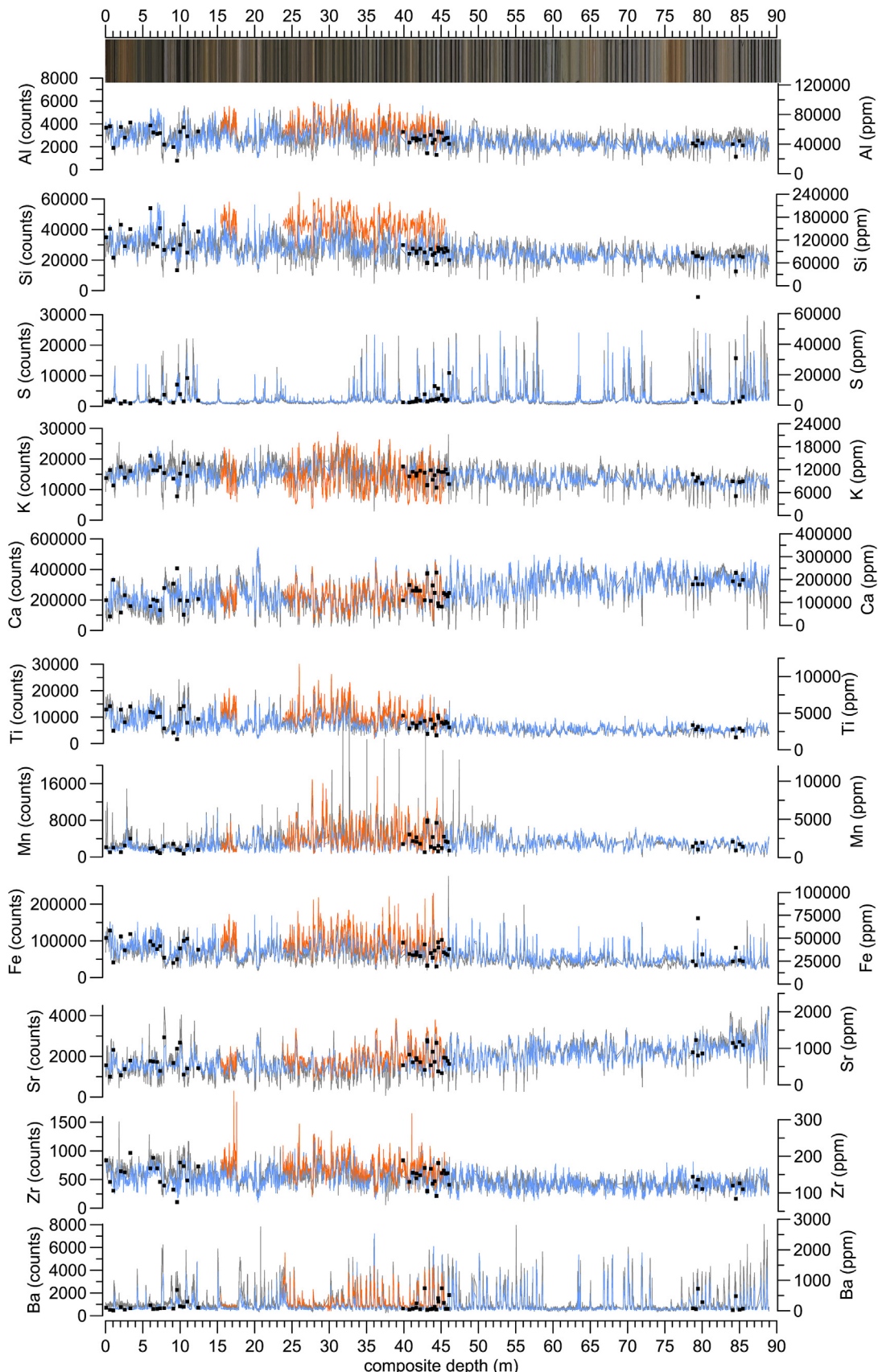
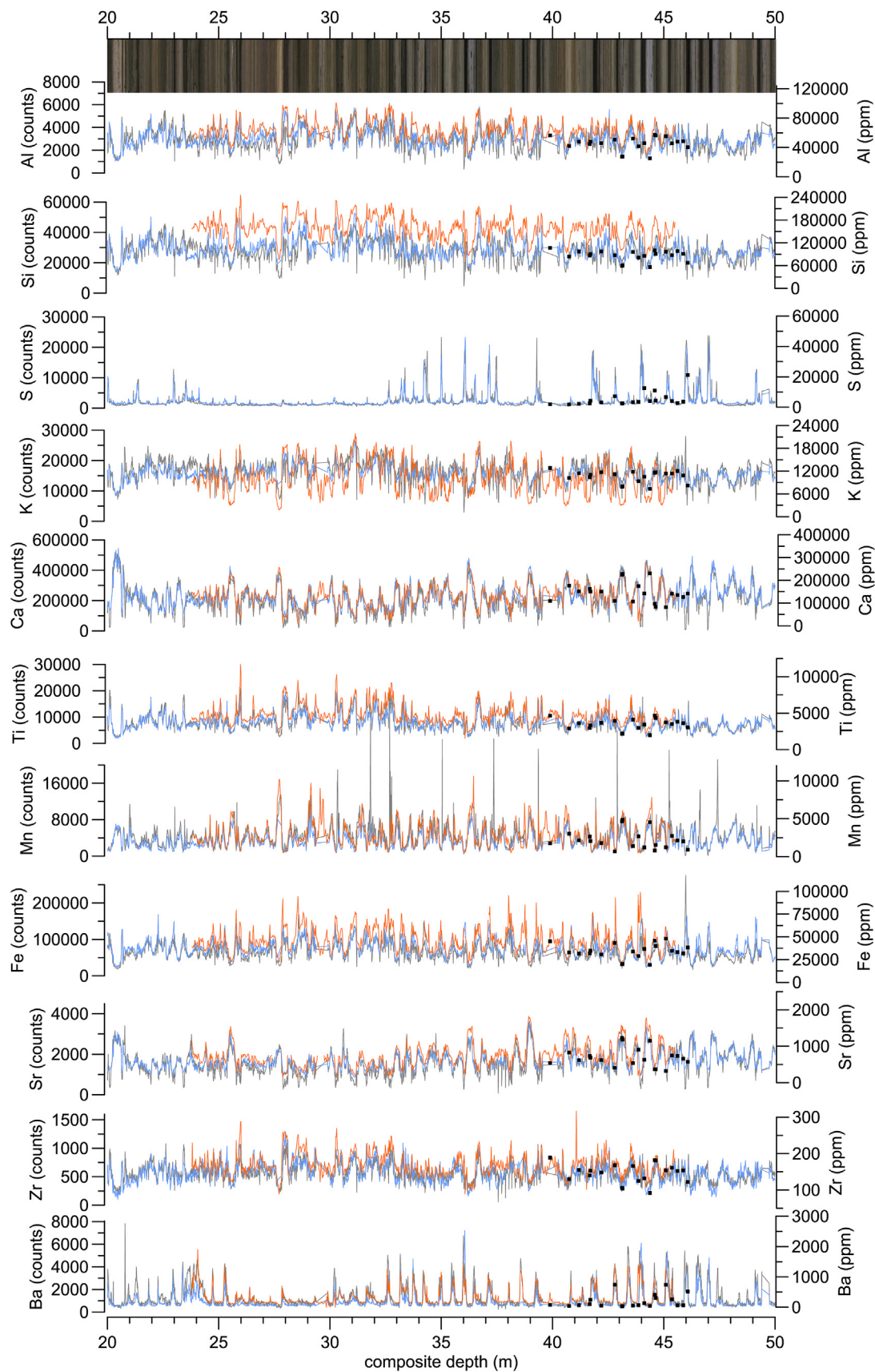


Fig. 2. ODP967 scanning and wave-length dispersive XRF results. Element counts (all data; grey) and calibrated concentrations (data after outlier removal; blue) from scanning XRF are shown with WD-XRF-derived element concentrations (black dots = this study; orange = Konijnendijk et al., 2014; 'TK2014'). (a) depicts the full 90 m, (b) shows details over the 20–50 m interval for comparison with the TK2014 record, which has been scaled to our composite depth scale.

**Fig. 2.** (continued).

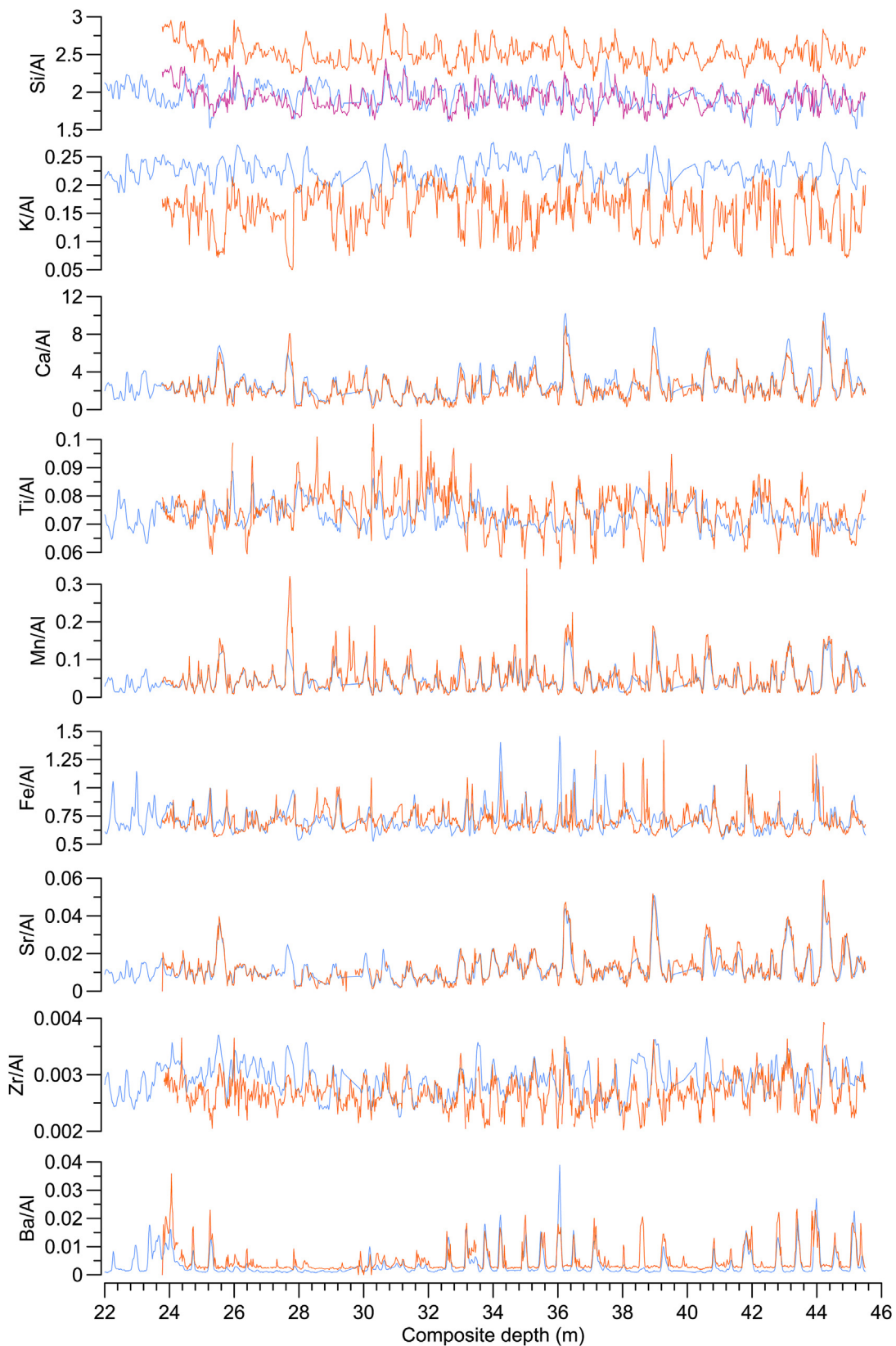


Fig. 3. ODP967 element/Al ratios based on fully-calibrated scanning XRF concentrations (blue) and WD-XRF (orange; TK2014, rescaled to our composite depth scale). The TK2014 Si/Al is also shown after offsetting by applying 0.5 (pink).

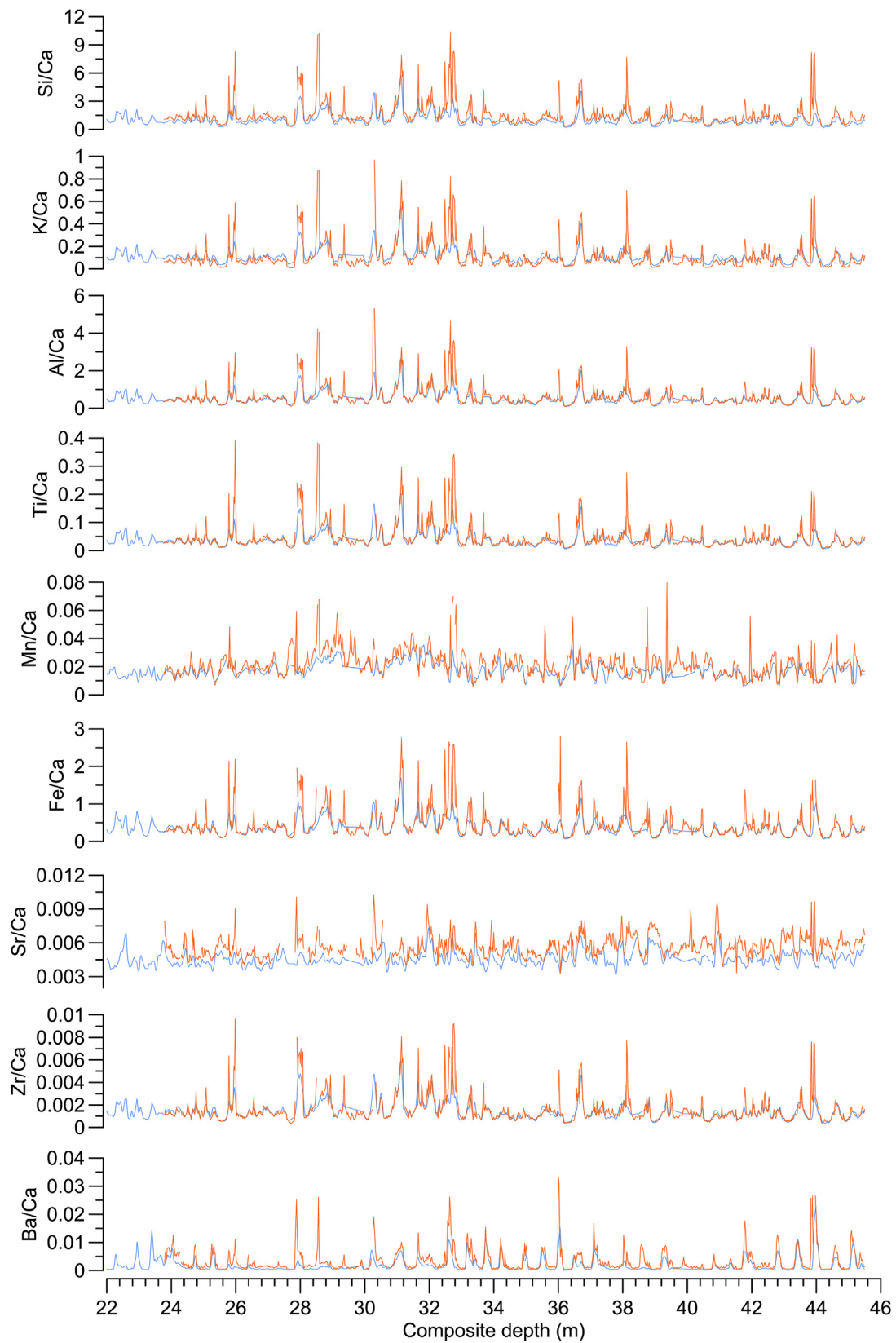


Fig. 4. ODP967 element/Ca ratios based on fully-calibrated scanning XRF concentrations (blue) and WD-XRF (orange; TK2014, rescaled to our composite depth scale).

between scanning and wavelength dispersive (WD)-XRF results may be expected. Yet our Sr/Ca record is nonetheless a close approximation of the TK2014 Sr/Ca in terms of relative variability, which – together with the other element/Ca records – suggests that all our element/Ca records are robust.

3.2. Principal component analysis

To aid interpretation of the downcore variability in geochemical composition, and in particular to try and identify a robust environmental signal for chronological purposes, a standardised principal component analysis (PCA) was performed on the calibrated scanning-XRF dataset. The advantage of applying this approach to geochemical compositional data is that it simultaneously quantifies relationships between all the elements in a dataset (as opposed to only focussing on single element profiles or element/element ratios), and therefore provides a more realistic picture of chemical compositional changes – hence environmental signals – over time. Also, detailed geochemical studies of ODP967 sapropels and their neighbouring sediments already exist (e.g., Van Os et al., 1991, 1994; Passier and De Lange, 1998; Nijenhuis et al., 1999; Wehausen and Brumsack, 2000), albeit for limited time intervals only. Our new XRF records therefore complement previous work and allow bulk chemistry changes to be investigated in a continuous sequence from 0 to 90 m composite depth (equivalent to ~3 My; see section 4).

Two principal components account for 79% of variance in our XRF data (Table 1), and this result is corroborated by PCA of the TK2014 dataset (Fig. 5a). The elemental composition of PC1 reveals that it reflects detrital versus biogenic inputs, while PC2 comprises elements associated with sapropels and their various redox states (Table 1) (Van Santvoort et al., 1997; Passier and De Lange, 1998;

Thomson et al., 1999). This interpretation is visually evidenced by strong similarity in downcore profiles of PC1 and Ti, and of PC2 and Ba (Fig. 5b). While Ba can be remobilised in sapropels following sulphate reduction and barite dissolution (Van Os et al., 1991, 1994), Ba nonetheless reliably tracks the position of sapropels, particularly those whose organic contents have been oxidised (Thomson et al., 1999). The finer detail in the PC2 signal compared to that of Ba through sapropel-poor intervals, suggests that PC2 provides a more comprehensive indication of sediment geochemical changes associated with sapropel deposition and preservation/oxidation. In other words, PC2 is likely to more accurately capture ‘ghost’ sapropels that have been poorly preserved.

Our interpretation of PC1 and PC2 can be further tested by comparing the residual signal between PC1 and PC2 with the ODP967 dust record of Larrasoña et al. (2003), and by comparing the residual signal between PC1 and the aforementioned dust record with PC2 (Fig. 5c). If PC1 represents the total detrital signal from riverine and aeolian inputs to this site, then removing the aeolian signal (~the dust record of Larrasoña et al., 2003), should reveal a residual riverine signal, which in this geographic setting and timeframe will predominantly reflect run-off from the Nile and wider North African margin; thus, the ‘riverine’ residual should correlate with our PC2 record. Similarly, if PC2 is an authentic proxy for African run-off, then the residual of PC1 (riverine + aeolian) and PC2 (riverine) should reflect aeolian inputs and can be tested by comparison with an independent record of aeolian inputs, such as the hematite dust record of Larrasoña et al. (2003). That record is based on environmental magnetic measurements of a different splice of ODP967 cores to our scanning XRF records, hence it is completely independent from our PC records. Due to the non-linear relationship between climate forcing and the environmental response recorded by the PC2 and dust records, both datasets were converted to standard normal distributions using an inverse transform sampling (ITS; see Emile-Geay and Tingley, 2016) prior to calculating residuals. In spite of some scaling offsets, overall a good agreement is observed between the residual signals and their respective ‘test’ records both in terms of their long-term trends and shorter-term fluctuations (Fig. 5c). For the dust and aeolian residual, $r^2 = 0.26$ and $p \approx 0$; for PC2 and the riverine residual, $r^2 = 0.12$ and $p \approx 0$. These correlations further support our interpretations of PC1 and PC2.

4. Chronology

The original ODP967 chronology (Sakamoto et al., 1998) was revised by Lourens et al. (2001) for the 2.2–3.2 Ma interval, and most recently by Konijnendijk et al. (2014) for the 0–1.4 Ma interval. These revisions, based on orbitally tuning Ti/Al variations, redressed some inconsistent insolation phasings from the original shipboard chronology. The 1.1–2.2 Ma interval was orbitally tuned by Lourens et al. (1998) based on shipboard identification of sapropels. Therefore, to maintain chronological consistency throughout our depth-splice, and to avoid potential age inaccuracies from the original shipboard chronology and visual identification of sapropel boundaries, we have constructed an age model specifically for our new splice (Table 2, Supplementary Fig. 5). The existing Ti/Al chronologies then provide a useful means to validate the age model adopted here.

For the 0–0.161 Ma interval, our chronology is constrained by radiometrically-based ages for the top and base of sapropels S1, S3, S4 and S5 (Grant et al., 2016), as well as two tephra layers (Table 2) that have been geochemically finger-printed and correlated to radiometrically-dated proximal deposits (Satow, 2012). For the 0.161–3.09 Ma interval, our sapropel/monsoon run-off proxy ('PC2', section 3) was tuned to precession minima with zero phase lag

Table 1

Results of principal component analysis of the ODP967 scanning XRF dataset. a) Element loadings for PC1 and PC2, where EE = everything else (see Section 2.2); b) scores for all components.

a	PC1	PC2
Al	0.34	-0.10
Si	0.32	-0.18
S	-0.01	0.58
K	0.32	-0.15
Ca	-0.34	-0.09
Ti	0.33	-0.11
Mn	-0.21	-0.24
Fe	0.29	0.20
Rb	0.34	-0.07
Sr	-0.31	-0.12
Zr	0.31	-0.12
Ba	0.06	0.60
“EE”	0.11	0.28

b	Score	%
PC1	8.08	62
PC2	2.27	17
PC3	1.04	8
PC4	0.59	5
PC5	0.38	3
PC6	0.20	2
PC7	0.18	1
PC8	0.13	1
PC9	0.07	1
PC10	0.03	0
PC11	0.02	0
PC12	0.00	0
PC13	0.00	0

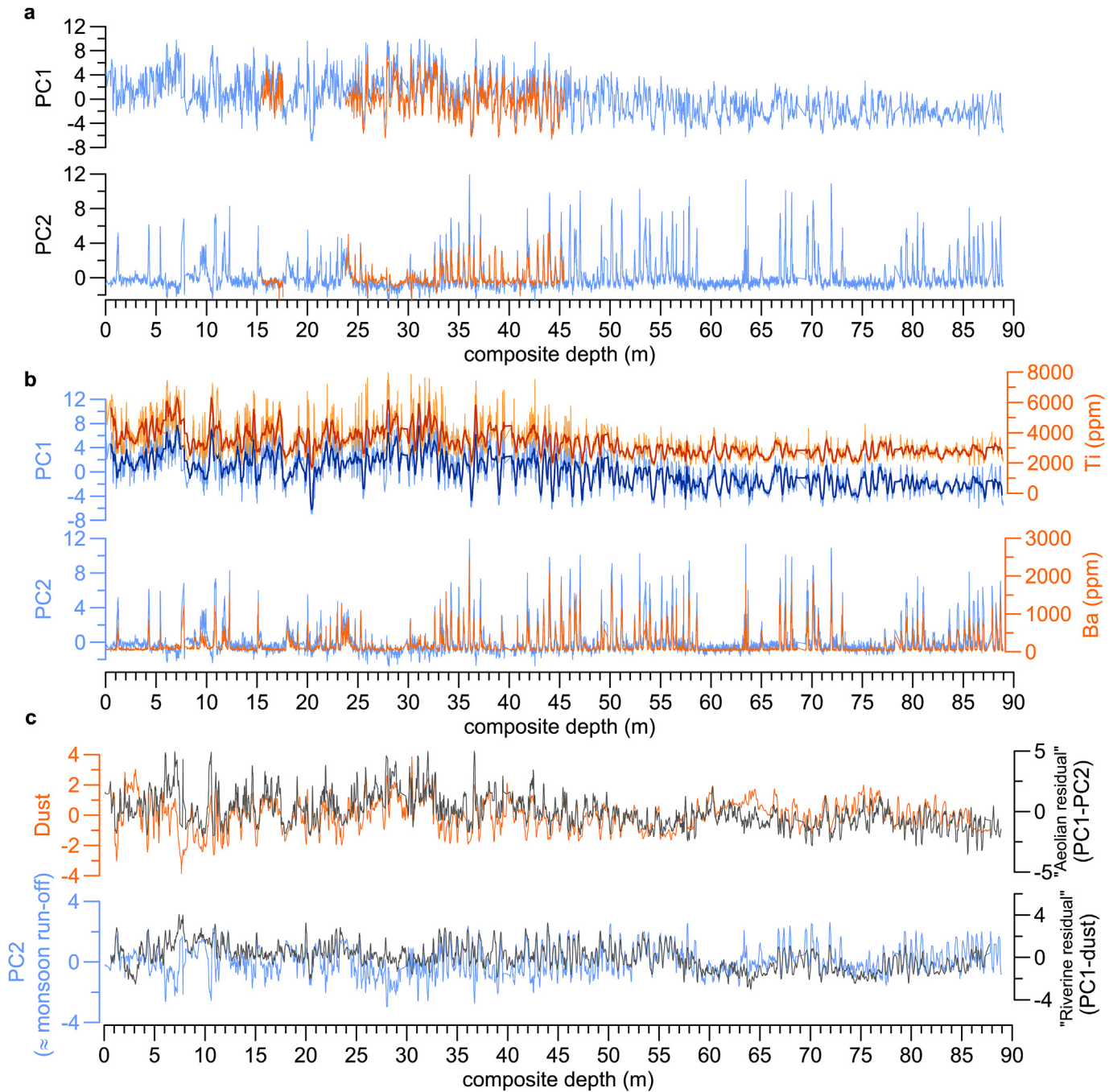


Fig. 5. Results of a principal component analysis of the ODP967 calibrated scanning XRF dataset. The first two principal components (PC1, PC2) account for 79% of variance in the dataset. a) PC1 and PC2 based on the calibrated scanning XRF dataset (blue) and on the TK2014 dataset (orange). b) PC1 and PC2 (blue) compared with the calibrated Ti and Ba records (orange). Darker lines in (b) are 21-point running averages. Note that Al, Si and Fe show similar variations as Ti (see Fig. 2b). c) ODP967 dust record (orange; Larrasoña et al., 2003; rescaled to our composite depth scale) and PC2 (blue) compared with the 'riverine' and 'aeolian' residuals (black; see Section 3.2 for details). The dust and PC records were transformed to standard normal distributions (section 3.2) to facilitate comparison with the residuals.

(below). While previous studies have used a 3-ky lag between inferred African monsoon maxima and precession minima (Lourens et al., 1996; Ziegler et al., 2010; Konijnendijk et al., 2014), this assumption has not been thoroughly tested for intervals older than the last glacial cycle. For the latter interval, Grant et al. (2016) observed a 2–3 ky precession-lag only after glacial terminations. This would imply little or no lag when monsoon maxima did not immediately follow a glacial termination, or prior to the onset of larger-amplitude glacial cycles ca 0.9 Ma. Similarly, Lourens et al.

(2001) suggested that late Pliocene and Early Pleistocene sapropels were directly in-phase with precession minima/insolation maxima. We therefore prefer not to introduce any untested assumptions about phasing, and thus assume a ± 3 ky age uncertainty throughout.

Regarding our tuning, spectral analysis of PC2 revealed a single, significant peak at frequencies of 1.75 ± 0.25 cycles/m (Supplementary Fig. 5a). Based on existing chronologies for ODP967 (Sakamoto et al., 1998; Lourens et al., 2001; Konijnendijk

Table 2

Age model for ODP967.

Depth (m)	Age (ky)	Event	Depth (m)	Age (ky)	Event
1.07	6.10	tS1	49.60	1568.00	s39
1.36	10.50	bS1	50.16	1606.26	s40
1.83	22.00	CR	50.66	1625.82	s41
4.12	80.80	tS3	51.20	1645.77	s42
4.38	85.80	bS3	52.37	1699.37	s43
5.28	101.80	tS4	52.93	1719.00	s44
5.50	107.80	bS4	53.46	1740.00	s45
7.50	121.50	tS5	53.99	1761.00	s46
7.80	128.30	bS5	55.11	1812.00	s47
8.96	161.00	KPT	55.64	1833.00	s48
9.72	175.63	S6	56.16	1854.28	s49
10.84	197.53	S7	57.28	1905.00	d
11.78	220.22	S8	57.86	1927.00	s51
12.30	241.35	S9	58.56	1948.17	s52
14.54	313.33	s*1	66.26	2077.00	ghost
15.12	334.82	s10	66.82	2098.00	s53
18.05	408.99	sb	67.39	2119.52	s54
20.08	485.46	s11	67.96	2140.00	s55
20.51	517.15	—	69.58	2212.62	s57
21.58	545.71	—	70.14	2234.53	s58
21.96	567.61	s*2	70.72	2255.66	s59
22.27	578.96	s*3	71.33	2281.09	ghost
23.50	621.60	s15	71.92	2305.34	s60
24.72	672.06	ghost	72.48	2327.25	ghost
25.29	692.19	s16	73.02	2348.00	s61
25.76	713.92	s17	73.57	2369.00	ghost
27.86	788.25	ghost	74.14	2400.58	ghost
30.21	864.93	s*4	75.14	2439.52	ghost
32.63	936.90	s18	75.50	2458.30	ghost
33.20	958.43	s19	75.81	2479.04	ghost
33.76	979.55	s20	76.27	2499.38	ghost
34.33	1001.46	s21	76.70	2522.07	ghost
34.92	1030.80	s22	77.25	2546.32	ghost
35.49	1051.92	s23	77.77	2570.00	ghost
36.05	1073.05	s24	78.85	2614.39	s63
36.58	1094.56	s25	79.40	2638.65	s64
37.12	1114.12	s26	79.96	2661.34	s65
38.67	1168.00	s27	80.50	2684.03	s66
39.27	1187.28	s28	81.05	2707.50	s67
40.80	1244.40	ghost	81.58	2730.19	ghost
41.32	1264.34	ghost	82.08	2754.05	ghost
41.86	1284.68	s29	83.05	2797.86	ghost
42.86	1318.00	s30	84.50	2875.32	s69
43.42	1337.28	s31	85.06	2905.11	s70
44.01	1359.41	s32	85.60	2927.35	s71
44.58	1380.14	s33	86.05	2947.78	s72
45.18	1401.00	s34	86.52	2970.70	s73
46.00	1432.17	s35	87.03	2993.86	s74
46.55	1453.30	s36	87.43	3019.68	s75
47.07	1473.64	s37	87.87	3041.20	s76
47.61	1494.77	ghost	88.26	3063.35	s77
49.06	1547.58	s38	88.70	3085.38	s78

Tephra horizons are CR (Cape Riva) and KPT (Kos plateau Tuff). Depths and ages of (ghost) sapropels relate to their mid-point, unless the top (t) and base (b) are specified.

et al., 2014), sedimentation rates were relatively constant through the Pleistocene, and ~90 m composite depth equates with ~3 My. The spectral peak in PC2 therefore relates to precession-band frequencies. This is not unexpected, given the well-established link between precession minima, North African monsoon maxima, and sapropel deposition (e.g., Rossignol-Strick, 1985; Rohling et al., 2015). This causal relationship has been the basis for previous astrochronologies for the Eastern Mediterranean (e.g., Hilgen, 1991; Lourens et al., 2004), including for ODP967 (Sakamoto et al., 1998).

We therefore applied a band-pass filter centred at 1.75 ± 0.25 cycles/m to the PC2 record, then – in most cases – synchronised peaks in the filtered PC2 to precession minima (Supplementary Fig. 5b). For a few sapropels associated with eccentricity minima, the original (unfiltered) PC2 signal was more clearly discernible

than its filtered signal, so in these cases tie-points were based on the original PC2 record. The resultant age model gives near identical depth-to-age scalings as the Ti/Al chronologies of Lourens et al. (2001) and Konijnendijk et al. (2014) (Supplementary Fig. 6). Similar agreement is also observed for the original shipboard chronology (Sakamoto et al., 1998) (Supplementary Fig. 6), although that chronology gives offsets with ours at ~0.65–0.9 Ma, ~1.55 Ma, and ~2.47 Ma. The Konijnendijk et al. (2014) chronology is also inconsistent with the original ODP967 shipboard chronology within the 0.65–0.9 Ma interval (Konijnendijk et al.'s chronology didn't extend beyond 1.4 Ma), but is consistent with revised, Mediterranean-based astrochronologies (Lourens, 2004; Lourens et al., 2004), which gives credence to our age model. Sapropels are poorly defined in this interval, as well as ca 1.5 Ma and 2.4–2.5 Ma where we also observe minor discrepancies (Supplementary Fig. 6). These times coincide with eccentricity minima and therefore weak precession minima, subdued monsoon maxima, and less developed sapropels. This can pose problems for tuning if the sapropel signal is not clearly identified. In contrast, the strong sapropel signal recorded by our PC2 record, and tight agreement between our chronology and that of Lourens et al. (2001), suggests that our age model is robust.

5. Discussion

5.1. Uncertainties in scanning XRF results

In spite of our robust multivariate log-ratio calibration (Supplementary Fig. S1) and well matched records from scanning and conventional XRF (Fig. 2), we observe deviations when calculating certain element ratios (namely, among Al, Si, K, Ti, and Zr; Figs. 3 and S4). The fact that variations in Ti, Si and K relative to Ca are consistent between scanning and conventional XRF, but not those relative to Al, suggests that the Al results may be at fault. Yet some element/Al ratios are clearly reliable (Fig. 3). This discrepancy warrants further investigation, since geochemical data are commonly presented in this way as a means of 'normalizing' element concentrations, and to compare transport pathways; e.g., Ti/Al at ODP967 has been used to approximate relative changes in aeolian (Ti) and riverine (Al) inputs to the site (e.g., Wehausen and Brumsack, 2000; Konijnendijk et al., 2014). In addition, presenting scanning XRF intensities as element ratios may reduce uncertainties associated with surface roughness, water content, and the sediment matrix (Weltje and Tjallingii, 2008). Considering therefore the sources of uncertainty in our calibrated XRF data, these primarily depend on uncertainties/limitations in XRF scanning, and on how well the selected reference samples represent the XRF scanning dataset. There is also the obvious methodological difference between WD-XRF on discrete, homogenised samples and XRF-scanning the surface micro-layer of an undisturbed sediment core, although in this study the strong correlation between reference and predicted concentrations (Supplementary Fig. S1) suggests methodological differences do not contribute significantly to the anomalous element/ratios.

Regarding reference-sample selection, a bi-plot of the calibrated XRF scanning results with the reference samples superimposed (Supplementary Fig. S7) demonstrates that our reference samples provide good coverage of the geochemical variance in the scanning XRF data, with the exception of extreme Ba and S values. Hence, it is unlikely that reference-sample selection is leading to extrapolation errors on the Al, Si, K, Ti and Zr calibrations. Focussing therefore on uncertainties in XRF scanning, these tend to be greatest for Al, which is typically at detection limits, has a shallow response depth in the sediment, and its fluorescence is rapidly attenuated (as is that of Si) in air/water (Rothwell and Croudace, 2015). For example, our

inauthentic Al and Si ratios may relate to variable water content – both within the sediment and under the protective film used for scanning (Kido et al., 2006; Tjallingii et al., 2007; Hennekam and De Lange, 2012; Bertrand et al., 2015). While we cannot rule this out, the scanned sections were relatively dry and compacted, having been open for several years prior to scanning. Also, MacLachlan et al. (2015) cited mixed results regarding the effects of water content on scanning counts.

Downcore changes in grain size and sediment porosity could also explain weaker correlations for Al, Si, K and Zr (e.g., Croudace et al., 2006; Weltje and Tjallingii, 2008; Rothwell and Croudace, 2015). Unfortunately, the effect of these variables on bulk geochemistry is difficult to isolate because there is inherent covariation between grain size, porosity, and lithology in clastic sediments. One approach is to use statistical models to separate the geochemical and geophysical components of bulk sediment measurements, but a comprehensive suite of measured parameters is needed to fully interpret results (Bloemsma et al., 2012). Regardless, mixed findings have been reported for the effects of grainsize on scanning XRF counts (Croudace et al., 2006; Tjallingii et al., 2007; Bertrand et al., 2015; MacLachlan et al., 2015). In any case, the fact that our calibrated scanning XRF data mostly correlate well with the raw counts and with an independent, wavelength-dispersive XRF dataset (Konijnendijk et al., 2014), implies that downcore geophysical changes (including water content and surface roughness) are not significantly affecting the authenticity of our scanning XRF results.

Spectrum-peak overlap can be an issue for K and Ti. High Ca and Ba intensities can interfere with the K and Ti spectra, respectively, in scanning XRF (e.g., Kuja et al., 2010; Rothwell and Croudace, 2015), although this is not always observed (Hennekam and De Lange, 2012). Calcium concentrations are high throughout ODP967, which may explain why the calibrated K record shows the poorest match with the TK2014 record (Fig. 2). Barium concentrations at ODP967 are highly variable and could therefore account for increased uncertainties on our Ti counts; this in turn would influence the correlation matrix in the calibration model, and hence the calibration results.

While any of the aforementioned sources of uncertainty may apply to our ODP967 results, no single explanation so far can account for uncertainties in ratios between Al, Si, K, Ti, and Zr. The common factor among these elements at ODP967 is that they are primarily associated with lithogenic sources. Our principal component analysis shows that it is the lithogenic elements that dominate geochemical variability at ODP967 (PC1 explains 62% of the total variance; Table 1). These elements have similar loadings in both PC1 and PC2 (the latter explains a further 17% of the variance), and their geochemical association can be visualized in a bi-plot (Supplementary Fig. S7). Thus, most of the variation among the lithogenic elements must be explained by PC3 and higher PCs, wherein the signal:noise ratio is much lower. It follows that ratios of lithogenic elements at ODP967 will be more strongly affected by their (relatively larger) uncertainties. Likewise, Ca and Sr have similar loadings in PC1 and PC2 (Table 1; Supplementary Fig. S7), so their relative uncertainties should also be larger. Fig. 4 suggests that this is indeed the case: our Sr/Ca ratios show the poorest match with the TK2014 data. Although values are small (order of 10^{-3}) and so larger offsets may be expected, Zr/Ca ratios are of similar magnitude yet show minimal offset to the TK2014 record.

In summary, the authenticity of element ratios at ODP967 most likely depends on the relative variation of the normalizing elements, although we cannot rule out scanning XRF uncertainties associated with spectral interference (affecting K, Ti), downcore changes in grain size and porosity (affecting Al, Si, K, Zr), and detection of Al (Rothwell and Croudace, 2015). More generally, our

results suggest that there is not a “one size fits all” approach to the use of element ratios based on scanning XRF, and such ratios should perhaps be used with caution if they cannot be rigorously supported by conventional XRF data. In particular – and most importantly – ratios among covarying, geochemically related elements may be unreliable when calculated from scanning XRF data, even when those data have been calibrated statistically using a multivariate log-ratio technique.

5.2. A new index of humidity/aridity

Our sapropel/monsoon proxy (PC2) may be interpreted in terms of past intervals of increased and widespread rainfall over the Sahara/North Africa or ‘GSPs’ (Larrasoña et al., 2013). However, this proxy is by definition less sensitive to drier periods when the monsoon did not penetrate as far north, so that there was little or no monsoon-related run-off into the Eastern Mediterranean and hence a lack of sapropel deposition. Comparison of the PC2 record with a previously published dust record from ODP967 (Larrasoña et al., 2003) reveals broadly inverse trends of different amplitude (Fig. 6a). Given that both records reflect a non-linear environmental response to climatic forcing, we converted each time-series to a standard normal distribution using an ITS (section 3.2) in order to facilitate a more meaningful comparison (Fig. 6b). Based on a Student's t-test where $t = 40.99$ and the effective degrees of freedom = 248 (Santer et al., 2000), correlation of the original and ITS-corrected dust and PC2 records ($r^2 = 0.219$ and 0.236, respectively) is highly significant ($p \approx 0$). While inverse covariation may be expected, given that both records should reflect changes in Saharan aridity and moisture, the underlying controls to these climate proxies are fundamentally different: PC2 is a more “wet sensitive” proxy that tracks run-off, while the ODP967 dust record is more “dry sensitive”, being strongly related to desertification of the Sahara. Such wet/dry sensitivities can explain differences between proxy signals of the same environmental changes, especially when strong non-linear feedback processes are at play, or when one or both records “saturates” (flat-lines) at high/low values (this is the case for both PC2 and the ODP967 dust record). A more holistic picture of climate variability may be attained if wet-sensitive and dry-sensitive proxy records are combined into a composite “wet-dry index”. To investigate this further, we have combined the ITS-corrected sapropel/monsoon index (PC2) and ODP967dust record (Larrasoña et al., 2003) to produce an integrated “wet-dry index” of Saharan/North African climate variability (Fig. 6c). This involved first detrending the dust record to remove a long-term increase over 3 My, and then quantitatively scaling its amplitude to that of PC2 in order to normalize the different proxy responses. This approach seems reasonable for these particular proxy records because they both pertain to North African monsoon variability, are from the same site, and both show more or less similar, but non-linear, trends.

Comparison of the ‘wet-dry index’ with Ti/Al records from ODP Sites 967/968 (Lourens et al., 2001; Ziegler et al., 2010; Konijnendijk et al., 2014) reveals strong agreement for 0–1.4 Ma ($r^2 = 0.53$, $p \approx 0$, based on ODP967 data only) and good agreement for 2.25–3.0 Ma ($r^2 = 0.34$, $p \approx 0$) (Fig. 6c). Ti/Al variations at these sites have been proposed to capture both humidity and aridity changes in North Africa relating to African monsoon variability (Wehausen and Brumsack, 2000), similar to our suggested wet-dry index. The fact that both records tend to pick out the same wet-dry fluctuations, and are based on completely different proxies and physical-process arguments, lends weight to both approaches. The potential advantage of our new wet-dry index is that it derives from a suite of geochemical (PC2) and environmental magnetic (the dust record) data that independently reflect changes in humidity and

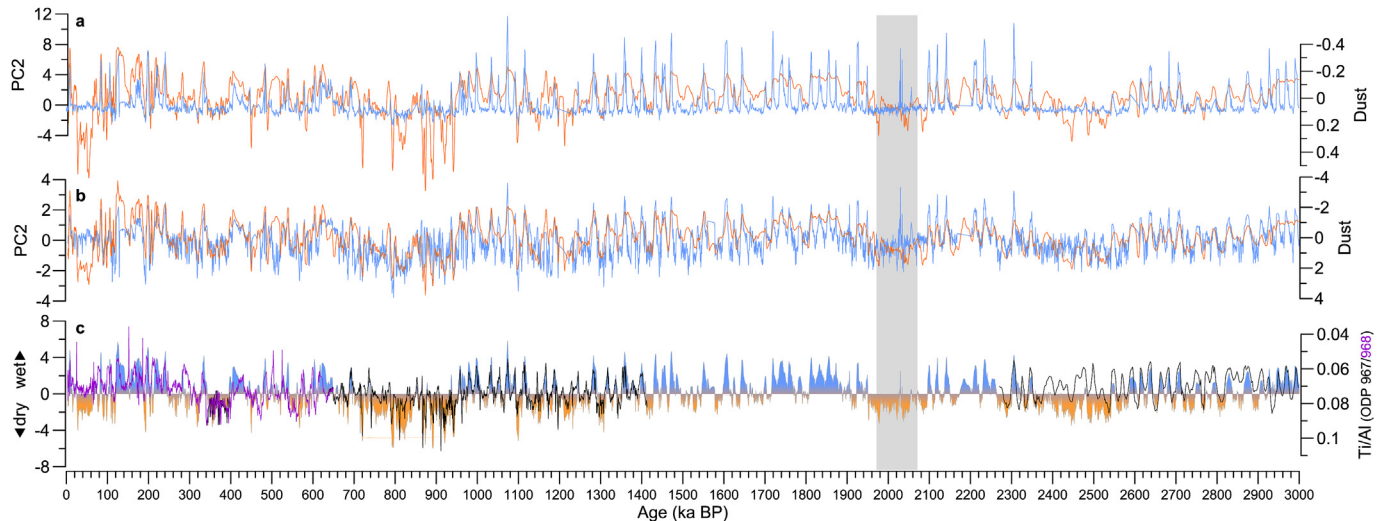


Fig. 6. Constructing a “wet-dry index” for ODP967. a) Comparison of the ODP967 PC2 record (blue; this study) with Larrasoña et al.’s (2003) ODP967 dust record (orange). Note the reverse y-axis for the dust record. b) As in (a) but after transforming both time-series to a standard normal distribution. c) The new “wet-dry” index, where shading denotes relatively more moisture (blue) or aridity (orange) based on the median of the index (see Section 5.2). Superimposed are Ti/Al records from: ODP Site 968 (purple; Ziegler et al., 2010; Konijnendijk et al., 2014), rescaled to the new chronology; ODP Site 967 (black; Lourens et al., 2001; Konijnendijk et al., 2014), rescaled to the new chronology; ODP Site 968 (purple; Ziegler et al., 2010; Konijnendijk et al., 2014), on the TK2014 chronology. A sediment slump interval is indicated (grey shading).

aridity (as opposed to changes in Ti relative to Al at ODP967, where both riverine and aeolian pathways supply Ti and Al).

5.3. Green Sahara periods over the last glacial cycle

Few continuous records of North African monsoon variability extend beyond the last glacial cycle with sufficient temporal resolution for useful comparison with our suggested wet-dry index. Furthermore, such comparisons can be misleading due to spatial and temporal variability in regional African palaeoclimate/environments, and inconsistencies among the timescales, resolution, and signal sensitivity of the compared proxy records (Gasse, 2000; Maslin et al., 2014). With this caveat in mind, we first focus on the last glacial cycle, comparing our wet-dry index with continuous, high-resolution marine records, and compiled continental data, of past humidity or monsoon changes in North Africa (below and Fig. 7). Then, in sections 5.4 and 5.5, we compare the wet-dry index with other evidence of enhanced humidity in North and East Africa over the last 3 My.

Regarding the last glacial cycle (Fig. 7), high-resolution marine records show strong similarities over this timeframe: all indicate increased moisture during MIS 1 and 5, despite offsets in exact timings (which can be partly attributed to age uncertainties). Continental records also support elevated Saharan humidity during MIS 5 (Fig. 7g) (as well as during MIS 1, see Drake et al., 2010). The evidence is more equivocal for MIS 3 ca 35–60 ka: the wet-dry index indicates significant aridity, while the other marine records imply at least some periods of increased humidity, which is consistent with the continental record (Geyh and Thiedig, 2008; Drake et al., 2013 and references therein). Larrasoña et al. (2013) investigated in detail the timing of North African wet periods over the last glacial cycle, using both marine and terrestrial records, and demonstrated a decreasing duration and time-transgressive onset of each wet period from south to north. Similar temporal offsets have been observed by other investigators (Kuechler et al., 2013; Shanahan et al., 2015). Latitudinal migration of the monsoon rainbelt may therefore explain inconsistencies among the records, including the MIS 3 disparity: i.e., monsoon rainfall didn't penetrate as far north at this time due to weaker insolation

maxima. However, a more humid interval during MIS 3 is also indicated by the Nile Fan record (Fig. 7d), so that there remain discrepancies among Eastern Mediterranean records that require another explanation (below).

The LC21 $\delta^{18}\text{O}$ residuals (Fig. 7a) predominantly reflect surface-water freshening in response to monsoon run-off (Grant et al., 2016), and these closely track the wet phases in our wet-dry index; Ti/Al fluctuations also generally follow the same trend (Fig. 7b). Among the Eastern Mediterranean marine records, therefore, the Fe record and to a lesser extent the kaolinite/chlorite record are most offset from our wet-dry index within MIS 3 (Fig. 7c–d). Kaolinite/chlorite variations in core MD40-SL71 are thought to reflect Saharan dust fluctuations, particularly as a function of dust-source availability in response to the intensity of humidity in the preceding interval (Ehrmann et al., 2017). Moderate kaolinite/chlorite values throughout MIS 3 show no clear trend and are not markedly different from those in MIS 1 and 2, unlike the other marine records. This disparity suggests that the kaolinite/chlorite record may be a convoluted signal of the availability of clay-bearing dust sources and intensity of dust fluxes. With respect to the Fe record from the Nile Fan, palaeo-Nile run-off was predominantly driven by East African and equatorial precipitation, whereas the LC21 and ODP967/968 records reflect an integrated monsoon/tropical precipitation signal from the Nile and wider North African margin (Rohling et al., 2015); this integrated signal is likely dominated by West African monsoon (WAM) variability (Paillou et al., 2009; Drake et al., 2013; Larrasoña et al., 2013). The African rainbelt shows strong spatial gradients over various timescales, reflecting the influence of both Atlantic and Indian Ocean climate dynamics (e.g., Gasse, 2000; Nicholson, 2009; Singarayer and Burrough, 2015), so discrepancies between the Nile Fan and other Eastern Mediterranean records may reflect different dynamics of the WAM and East African precipitation.

A third explanation for the more diverse MIS 3 reconstructions is a change in dust fluxes. Globally, glacial periods are generally associated with higher dust fluxes (e.g., Winkler et al., 2008), in line with the ODP967 dust record and hence with the wet-dry index. Relatively high Ti/Al values at this time (Fig. 7b) are also consistent with more aeolian than riverine inputs to the Eastern

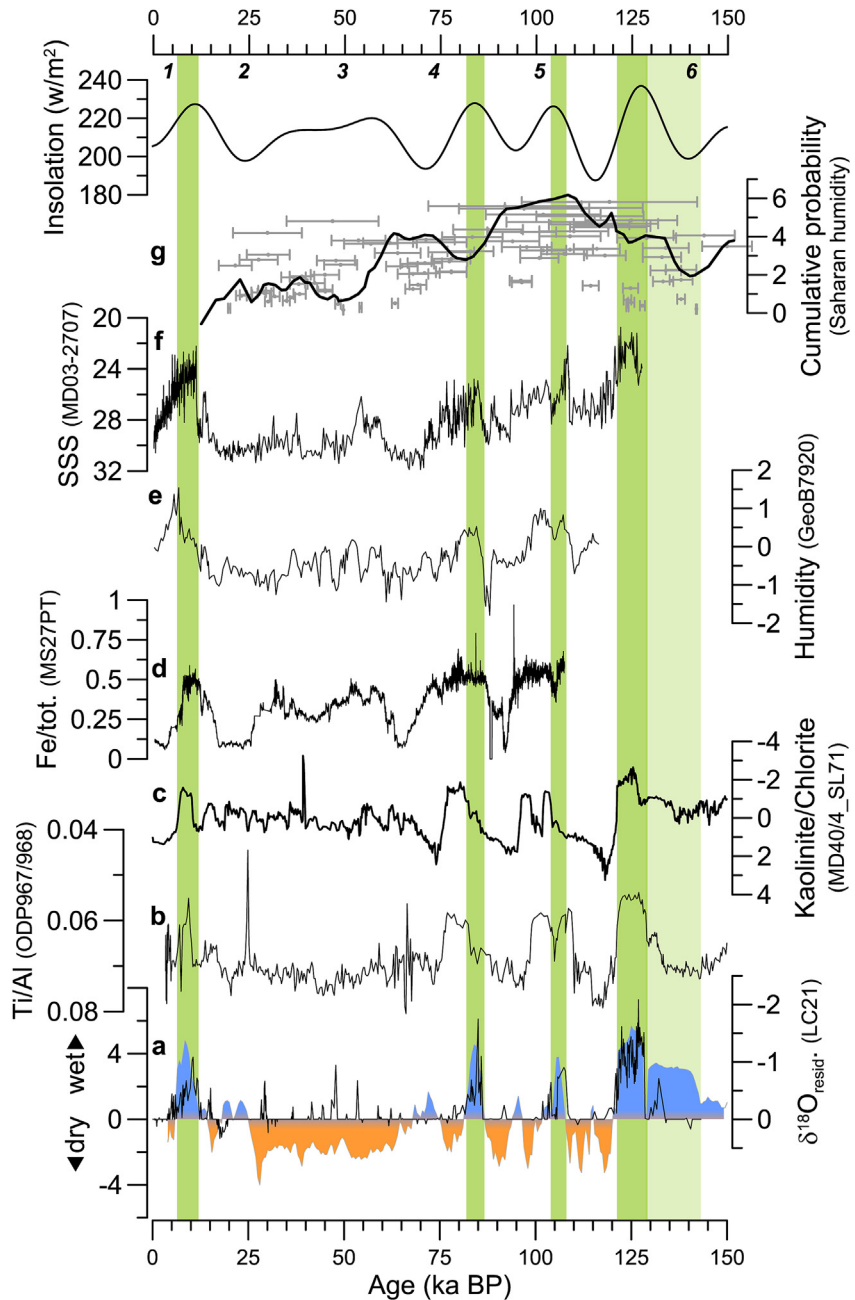


Fig. 7. Proxy records of Northwest African moisture variability spanning the last glacial cycle. See Fig. 1 for core locations. a) wet-dry index from ODP967 (blue/orange; this study) and the residual $\delta^{18}\text{O}$ record from core LC21, Eastern Mediterranean (black; Grant et al., 2016), b) Ti/Al record from an ODP967/968 splice (Konijnendijk et al., 2014), c) kaolinite/chlorite variations in core MD40/4–SL71, Eastern Mediterranean (Ehrmann et al., 2017), transformed to a standard normal distribution, d) Fe record from Nile Fan core MS27PT (Revel et al., 2010), e) XRF-derived humidity index from core GeoB7920 off Northwest Africa (Tjallingii et al., 2008), f) sea surface salinity (SSS) reconstructed from Ba in core MD03-2707, off west equatorial Africa (Weldeab et al., 2007), g) continental evidence (primarily lacustrine deposits) of intervals of increased Saharan humidity (grey points with 1σ error bars, and their cumulative probability distribution; Drake et al., 2013). Marine isotope stages 1–6 and the subtropical insolation gradient (23°N – 23°S on June 21st) are also shown. Green shading indicates intervals where an inferred increase in humidity is common to all records; paler green shading is tentative, as only a few marine records extend that far.

Mediterranean. In contrast, the more ‘wet sensitive’ proxies, such as run-off indicators or lacustrine deposits, are less accurate tracers of dust fluxes. Studies of loess sequences in the Negev desert (Israel) suggest that Arabian dust fluxes to the Eastern Mediterranean significantly increased from ~180 ka onwards (Amit et al., 2011; Ben Israel et al., 2015), in which case the ODP967 dust record (hence the wet-dry index) may be biased by Arabian dust inputs and thus suggest more aridity than records off Northwest Africa.

Studies of pollen and plant-wax $\delta^{13}\text{C}$ and δD in cores offshore NW Africa can shed light on Saharan-Sahelian humidity/aridity

changes during MIS 3. Kuechler et al. (2013) inferred relatively arid conditions through most of MIS 3, with an increase in humidity ca 35 ka (ODP Sites 658/659, 18 – 21°N); Niedermeyer et al. (2010) also inferred a wet phase in late MIS 3 (38–28 ka), although their record did not extend further back in time (core GeoB9508-5, 15°N); and Castañeda et al. (2009) inferred a more humid phase at ~50–45 ka (core GeoB9528-3, 10°N). Interpretation of plant-wax $\delta^{13}\text{C}$ and δD in terms of humidity/aridity changes is not straightforward, however (see discussion in Feakins, 2013; Kuechler et al., 2013). For example, $\delta\text{D}_{\text{wax}}$ may be biased by vegetation changes (Feakins,

2013), or in the case of northwest Africa, disparate trends between proxy records may relate to core locations and corresponding latitudinal differences in vegetation cover (Kuechler et al., 2013). Added to this, a review of African rainbelt dynamics over the last glacial cycle which included model simulations, demonstrated significant regional variability linked to multiple forcing mechanisms over varying timescales (Singarayer and Burrough, 2015). It is perhaps not surprising, then, that during MIS 3 in particular – a period of pronounced millennial-scale fluctuations between climate extremes (Voelker, 2002) – there is such ambiguity when considering multiple African humidity reconstructions.

In light of these complexities, the consistent evidence for increased moisture in Northwest Africa during MIS 1, 5a, 5c and 5e is highly convincing (Fig. 7; see also Drake et al., 2013; Larrasoña et al., 2013, and references therein). This evidence is supported by hydraulic modelling of potential North African palaeo-river channels under MIS 5e climate conditions (Coulthard et al., 2013). Satellite imagery of a palaeo-river system draining the northwest African margin (Skonieczny et al., 2015) and sedimentary features in the same area (Antobreh and Kastel, 2006; Wien et al., 2006; Skonieczny et al., 2015) also attest to GSPs. Importantly, the fact that our ‘wet-dry index’ captures elevated humidity in MIS 1, 5a, 5c and 5e confirms that it is a reliable proxy of GSPs. The purported link between GSPs and sapropel deposition in the Eastern Mediterranean (Larrasoña et al., 2013) therefore appears to be robust, given that our sapropel-sensitive PC2 record contributes to the wet-dry index. The typically shorter duration of sapropels, and of our inferred ‘wet’ intervals, relative to other records of Northwest African humidity, is most plausibly explained if the wet-dry index tracks African monsoon variability at its northernmost extent. We therefore further surmise that the wet-dry index offers a minimum estimate for the duration of GSPs over the last 3 My.

5.4. Green Sahara periods over the past 3 My

There are few continuous records of Saharan palaeoclimate variability to compare with our wet-dry index over the 0–3 Ma interval. Apart from the ODP967 Ti/Al record (Fig. 6), only a dust record from offshore Northwest Africa (ODP Site 659; Tiedemann et al., 1994) is sufficiently long. Visually, the two records appear to show some notable differences (Fig. 8), although non-linear scaling offsets between the records may at least partly explain this. However, statistical analysis of the same ODP Site 659 dust record, the ODP967 dust record used in our wet-dry index (Larrasoña et al., 2003), and an Arabian dust record from ODP Sites 721/722, revealed differences between all three sites over various timeframes (Trauth et al., 2009), thereby highlighting inter-regional variability in Sahara-Arabian dust fluxes over the past 3 My. Dust accumulation in marine cores is related to the availability of source material (which in turn depends on prior humidity), abrasion, and transport of aeolian particles to the core sites, and these processes particularly depend on wind strength and direction (e.g., Zabel et al., 1999, 2001). Thus, a proxy sensitive to changes in both aridity and humidity (i.e., our wet-dry index) may not directly correlate with a dust-flux record if the latter reflects changes in wind strength and direction in addition to aridity.

For Saharan/North African humidity indicators, the continental record is best constrained for the last ~400 ky (see Geyh and Thiedig, 2008; Drake et al., 2013; for detailed reviews). Over this period, there is a very broad age distribution of samples indicative of increased moisture, and most of these ages overlap within uncertainties (Figs. 7 and 8). Nonetheless, the median of these ‘humid’ intervals tends to coincide with wetter intervals on our index. For example, evidence includes radiometrically dated lake deposits in Egypt (East Sahara) at 320–250, 240–190, 155–120, 90–65, and 10–5

ka (Szabo et al., 1995), and in Libya (North Sahara) at 380–290, 260–205, 140–125, 12.5–6 ka (Geyh and Thiedig, 2008); these intervals match peak density distributions of compiled data on Saharan palaeo-humidity (Fig. 8).

The large spread of ages among the continental data may reflect regional climatic/environmental heterogeneity across North Africa, latitudinal migration of the African monsoon rainbelt, and/or less accurate datings in older studies. For example, Armitage et al. (2007) noted significant offsets between their OSL datings of Libyan lacustrine deposits (100–110 ka) and Petit-Maire et al’s (1980) U-series datings of the same samples (~135 ka, ranging from 40 ± 2 ka to 165 ± 17 ka). Prior to 0.4 Ma, the only published evidence of Saharan humidity (to our knowledge) that we can usefully compare with our index consists of ^{10}Be -dated lake deposits from the northern Chad Basin, at 3 ± 0.19 Ma and 2.31 ± 0.21 Ma (Lebatard et al., 2010). In spite of the large uncertainties, the most likely ages coincide with wetter intervals according to our index (Fig. 8).

5.5. Saharan and East African humidity over the last 3 My

Given the dearth of detailed records of Saharan/West African palaeoclimate variability over the past 3 My, we also compare our wet-dry index with evidence of past East African humidity (Fig. 8). Many lines of evidence suggest that the Holocene African Humid Period (AHP) extended to East Africa north of ~10°S (e.g., Street and Grove, 1976; Gasse, 2000; Tierney et al., 2008, 2011; Berke et al., 2012; Tierney and deMenocal, 2013; Costa et al., 2014). The latitude of this ‘hinge point’, nominally distinguishing between predominantly northern- and southern-hemisphere modes of climate variability, largely depends on the position of the ITCZ and Congo Air boundary (CAB), and both migrate over seasonal to orbital timescales (e.g., Nicholson, 1996, 2000; Broccoli et al., 2006; Costa et al., 2014; Schneider et al., 2014). The ITCZ tends to shift meridionally towards the hemisphere of greatest radiative forcing, while the position of the CAB is determined by the confluence of low-level westerly and easterly air streams and topography (the Kenyan and Ethiopian Highlands). As a result, palaeoprecipitation reconstructions for tropical East Africa are relatively complex, such that both symmetrical and asymmetrical moisture trends north and south of the hinge zone have been observed (e.g., Barker et al., 2002; Garcin et al., 2006; Castañeda et al., 2007; Konecky et al., 2011; Otto-Bliesner et al., 2014; Singarayer and Burrough, 2015; Johnson et al., 2016). Lake Malawi appears to intersect or lie just south of the southernmost limit of this hinge zone: today, precipitation follows austral insolation, and palaeohumidity reconstructions (implying low lake levels during the early Holocene) suggest this was also the case over orbital timescales (Castañeda et al., 2007; Konecky et al., 2011). Equally, detailed lake level reconstructions suggest intermittent highstands during the Holocene (Johnson et al., 2016, and references therein). Such apparently conflicting observations may be reconciled if moisture transport to the region was complex (Lyons et al., 2015; Singarayer and Burrough, 2015).

In the following comparison, therefore, we only consider i) records extending beyond the last glacial period, since the Holocene East African Humid period is detailed in other studies, ii) sites as far south as Lake Malawi, and iii) published records that allow us to robustly identify and depict, in conjunction with our index, when humidity increased in both North/West and tropical East Africa. Our aim is to test whether East African Humid Periods prior to the Holocene AHP were synchronous with Green Sahara periods (GSPs). Long-term trends in African climate variability over the last 3 My and beyond have already been reviewed in detail by deMenocal (2004), Trauth et al. (2009) and Maslin et al. (2014), who

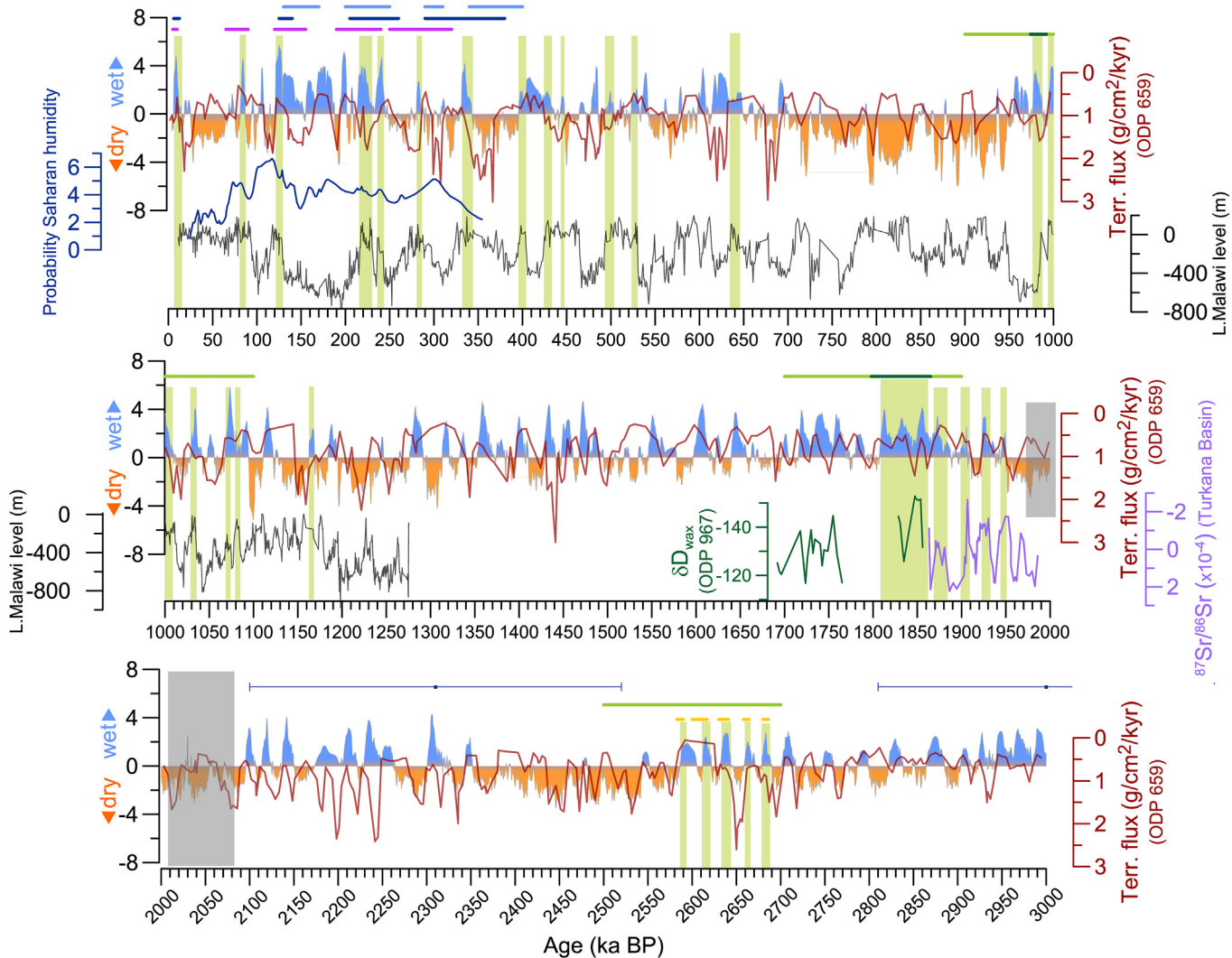


Fig. 8. Evidence for Northwest and East African humid intervals over the past 3 million years. See Fig. 1 for site locations. The ODP967 wet-dry index (blue/orange; this study) is shown with time-series of: terrigenous fluxes at ODP Site 659 (red; Tiedemann et al., 1994); probability density curve for Saharan humidity (dark blue; Drake et al., 2013); Lake Malawi lake level (grey; Lyons et al., 2015); plant-wax δD in ODP967 (green; Rose et al., 2016); $^{87}\text{Sr}/^{86}\text{Sr}$ in fossil fish from the Turkana Basin (purple; Joordens et al., 2011). Horizontal bars denote the timing of: East Saharan lacustrine deposits (pink; Szabo et al., 1995); North Saharan lacustrine deposits (dark blue; Geyh and Thiedig, 2008); clusters of North Saharan lacustrine deposits based on published data (pale blue; Geyh and Thiedig, 2008); East African humid intervals inferred from Rift basin records (green), including well-constrained lake periods in the Olorgesailie and Olduvai Basins ca 0.98 and 1.8–1.86 My respectively (dark green; Trauth et al., 2009); Kenyan Rift basin diatomites (yellow; Deino et al., 2006; Kingston et al., 2007); ^{10}Be -dated lake facies from the Chad basin (blue squares $\pm 1\sigma$ error bars; Lebatard et al., 2010). Green shading indicates intervals where increased humidity is indicated by both the wet-dry index and East African records, hence the timing of potentially widespread humidity across Northwest/Saharan and East Africa. A sediment slump in ODP967 is indicated (grey shading).

also considered mechanisms of climate change. That is not the focus of this study. Our study also differs from these reviews in that Trauth et al. (2009) focussed on dust records only, Maslin et al. (2014) were concerned with East African rather than Saharan records, and deMenocal's (2004) review pre-dates the small but growing number of well-dated and better-resolved palaeoclimate records from the region.

The longest and best resolved record of humidity changes in East Africa is from Lake Malawi (Fig. 8), where a lake level index has been derived from total organic carbon, $\delta^{13}\text{C}$ of organic matter, bulk density, carbonate abundance, and colour reflectance (Lyons et al., 2015) (Fig. 8). Similarities and offsets are observed between inferred lake highstands and wetter intervals on our index. (As the lake chronology is less well-constrained in the interval 75–590 ka, we focus only on humidity intervals lasting multi-millennia or longer). Where there is coherence between the records, it tends to be

supported by reduced dust fluxes at ODP Site 659 (Fig. 8), which implies a degree of covariation between the West African monsoon (WAM) and tropical Southeast African precipitation. The latter is strongly related to Indian Monsoon (IM) dynamics, so covariation of WAM and IM dynamics is not unexpected if the notion of a coherent 'global monsoon' variability is valid over orbital time-scales (e.g., Caley et al., 2011; Wang et al., 2014; Jiang et al., 2016). In addition, rising greenhouse gases and millennial-scale AMOC (Atlantic meridional overturning circulation) variability may explain in-phase precipitation trends between North/West and tropical Southeast Africa (Otto-Bliesner et al., 2014). For example, simulations show that a resumption of AMOC and subsequent warming in the North Atlantic ca 14.7 ka led to an increase in precipitation over North Africa and also, via atmospheric teleconnections, to warming over the Indian Ocean and an attendant increase in Southeast African precipitation (Otto-Bliesner et al.,

2014). Previous experiments and palaeodata from the WAM and IM regions support such a link between AMOC and moisture variability (e.g., Wang et al., 2001; Mulitza et al., 2008; Collins et al., 2013; Kageyama et al., 2013; Deplazes et al., 2014). At the same time, disparate trends between our index and inferred levels of Lake Malawi (Fig. 8) may be expected given that the lake receives peak rainfall in austral summer, and that much of its catchment lies south of the north-south 'hinge zone'.

In contrast, much closer agreement is observed between our index and $^{87}\text{Sr}/^{86}\text{Sr}$ ratios of lacustrine fish fossils from the Turkana Basin (Fig. 8), which reflect monsoon-driven rainfall variability between ~2 and 1.85 Ma (Joordens et al., 2011). A persistence of the same trend appears to be reflected (discontinuously) in a leaf-wax δD record from ODP967 between 1.85 and 1.7 Ma (Rose et al., 2016), although this may also reflect WAM variability. Diatomite deposition in the Kenyan Rift between 2.68 and 2.58 Ma (Deino et al., 2006; Kingston et al., 2007) also matches our inferred wet intervals (Fig. 8). Just south of the equator at Olduvai Gorge, precessional cyclicity of $\delta^{13}\text{C}_{n\text{-alkane}}$ -derived vegetation changes has also been observed within the 1.9–1.8 Ma interval (Magill et al., 2013).

A detailed compilation of sediment records from the East African Rift System, spanning 3 My and $\sim 5^\circ\text{N}$ to $\sim 3^\circ\text{S}$, offers further insights into potential East African wet phases (Trauth et al., 2005) (Fig. 8). Three extended periods of elevated moisture in East Africa have been inferred at 2.7–2.5, 1.9–1.7, and 1.1–0.9 Ma (see Trauth et al., 2005, and references therein). While these timings appear to coincide with pockets of repeated wet intervals on our index, the index also indicates humid periods outside the Trauth et al. (2005) intervals. The primary control of lake phases in the EAR system is accommodation space, which is determined by tectonic activity and sedimentation, so inferred lake intervals may not exactly equate with elevated moisture. Yet precession-scale climate variability also influences the lake water budgets (e.g., Feibel, 2011), and where the EAR records have precession-scale age control there is excellent agreement with our index (e.g., in the Turkana, Baringo, and Olorgesailie Basins, Fig. 8).

Given the latitudinal and topographic extent (hence, moisture variability) of the EAR system, and the influence of tectonics on lake phases, the overall agreement between the rift basin evidence and our wet-dry index is remarkable, and would suggest many periods of in-phase moisture variability across West and East Africa. Whether these intervals are termed 'African Humid Periods' (AHPs) is probably subjective. Strictly, the AHP refers to the early Holocene in North Africa. A reference to more generic AHPs could be misleading when there is clearly a high degree of inter- and intra-regional moisture variability over varying timescales (e.g., Gasse, 2000; deMenocal, 2004; Maslin et al., 2014; Singarayer and Burrough, 2015). Equally, recognizing intervals that are characterized by elevated humidity across large tracts of both West and East Africa is useful for studies of hominin evolution and dispersals, as well as for understanding large-scale (palaeo)climate dynamics. As more records become available with higher resolution and chronological integrity, particularly for intervals where there is currently a dearth of detailed information (i.e., 1.7–1.3, 2.5–2.0, and 0.9–0.4 Ma, Fig. 8), the extent of such pan-African Humid periods can be better defined.

6. Conclusions

The combined ODP Site 967 XRF dataset from this study and Konijnendijk et al. (2014) provides a unique opportunity to examine the accuracy of scanning XRF records over a relatively long time interval in unprecedented detail. Our results demonstrate that even when element counts from scanning XRF authentically represent downcore variations in element concentrations, certain

element ratios based on scanning XRF may not accurately reflect the same element ratios derived from conventional geochemical analysis. We observed this inauthenticity in some ratios despite thoroughly calibrating element counts into concentrations using the advanced multivariate log-ratio technique, and removing outliers after calibration. This suggests the need for a 'reality check' when interpreting scanning XRF records, and raises issues for the now common application of scanning XRF element ratios in downcore correlations and stratigraphy. At ODP967, ratios between elements from similar sources (e.g., Ti/Al, Sr/Ca) show less authentic signals compared to those from conventional XRF.

Principal component analysis of our calibrated XRF data yielded a sapropel/monsoon run-off proxy that can be used to identify ghost sapropels at ODP967 and establish orbital chronologies. Furthermore, by combining this sapropel proxy – which is sensitive to monsoon run-off into the Eastern Mediterranean – with a published dust record from the same site, we have produced a new index of changes in relative humidity and aridity in Northwest Africa. This index appears to give a reliable indication of the occurrence of Green Sahara Periods over the last 3 million years, and a minimum estimate of their duration. Together with well-dated, published records of humidity changes in East Africa, the index allows us to highlight intervals where both North/West and East Africa likely experienced elevated humidity. Documenting such pan-African humid episodes may be of considerable importance for efforts to understand human evolution/migrations.

Acknowledgments

We thank Walter Hale and Vera Lukies at Marum for their assistance with core scanning and sampling, and Roy Wilkens for help with IGOR Pro software. This work was supported by Australian Research Council Australian Laureate Fellowship FL1201000050 (EJR), and by the Deutsche Forschungsgemeinschaft (We5479-1) (TW). We thank Jess Tierney and Rik Tjallingii for helpful feedback on the manuscript.

Appendix. ASupplementary data

Supplementary data related to this article can be found at <http://dx.doi.org/10.1016/j.quascirev.2017.07.005>.

References

- Amit, R., Enzel, Y., Crouvi, O., Simhai, O., Matmon, A., Porat, N., McDonald, E., Gillespie, A.R., 2011. The role of the Nile in initiating a massive dust influx to the Negev late in the middle Pleistocene. *Geol. Soc. Am. Bull.* 123, 873.
- Antobreh, A.A., Kastel, S., 2006. Morphology, seismic characteristics and development of Cap Timiris Canyon, offshore Mauritania: a newly discovered canyon preserved-off a major arid climatic region. *Mar. Petroleum Geol.* 23, 37–59.
- Armitage, S.J., Drake, N.A., Stokes, S., El-Hawat, A., Salem, M.J., White, K., Turner, P., McLaren, S.J., 2007. Multiple phases of north African humidity recorded in lacustrine sediments from the Fazzan basin, Libyan sahara. *Quat. Geochron 2*, 181–186.
- Barker, P., Telford, R., Gasse, F., Thevenon, F., 2002. Late Pleistocene and Holocene palaeohydrology of lake Rukwa, Tanzania, inferred from diatom analysis. *Paleogeogr. Palaeoclimatol. Palaeoecol.* 187, 295–205.
- Ben Israel, B., Enzel, Y., Amit, R., Erel, Y., 2015. Provenance of the various grain-size fractions in the Negev loess and potential changes in major dust sources to the Eastern Mediterranean. *Quat. Res.* 83, 105–115.
- Berke, M.A., Johnson, T.C., Werne, J.P., Grice, K., Schouten, S., Sinnenberg Damsté, J.S., 2012. Molecular records of climate variability and vegetation response since the late Pleistocene in the lake Victoria basin, east Africa. *Quat. Sci. Rev.* 55, 59–74.
- Bertrand, S., Hughen, K., Giosan, L., 2015. Limited influence of sediment grain size on elemental XRF core scanner measurements. In: Croudace, I.W., Rothwell, R.G. (Eds.), *Micro-xrf Studies of Sediment Cores, Developments in Paleoenvironmental Research*, vol. 17. http://dx.doi.org/10.1007/978-94-017-9849-5_19.
- Bloemsma, M.R., Zabel, M., Stuut, J.B.W., Tjallingii, R., Collins, J.A., Weltje, G.J., 2012. Modelling the joint variability of grain size and chemical composition in sediments. *Sediment. Geol.* 280, 135–148.
- Broccoli, A.J., Dahl, K.A., Stouffer, R.J., 2006. Response of the ITCZ to northern

- hemisphere cooling. *Geophys. Res. Lett.* 33, L01702. <http://dx.doi.org/10.1029/2005GL024546>.
- Caley, T., Malaïzé, B., Revel, M., Ducassou, E., Wainer, K., Ibrahim, M., Shoeib, D., Migeon, S., Marieu, V., 2011. Orbital timing of the Indian, East Asian and African boreal monsoons and the concept of a 'global monsoon'. *Quat. Sci. Rev.* 30, 3705–3715.
- Calvert, S.E., Fontugne, M.R., 2001. On the late Pleistocene-Holocene sapropel record of climatic and oceanographic variability in the eastern Mediterranean. *Paleoceanography* 16, 78–94.
- Castañeda, I.S., Werne, J.P., Johnson, T.C., 2007. Wet and arid phases in the Southeast African tropics since the last glacial maximum. *Geology* 35, 823–826.
- Castañeda, I.S., Mulitza, S., Schefuß, E., Lopes dos Santos, R.A., Sinnighe Damsté, J.S., Schouten, S., 2009. Wet phases in the Sahara/Sahel region and human migration patterns in North Africa. *Proc. Natl. Acad. Sci. U. S. A.* 106 (48), 20159–20163.
- Collins, J.A., Govin, A., Mulitza, S., Heslop, D., Zabel, M., Hartmann, J., Röhle, U., Wefer, G., 2013. Abrupt shifts of the sahara–Sahel boundary during Heinrich stadials. *Clim. Past* 9, 1181–1191. <http://dx.doi.org/10.5194/cp-9-1181-2013>.
- Costa, K., Russell, J., Konecky, B., Lamb, H., 2014. Isotopic reconstruction of the African humid period and Congo air boundary migration at lake Tana, Ethiopia. *Quat. Sci. Rev.* 83, 58–67.
- Coulthard, T.J., Ramirez, J.A., Barton, N., Rogerson, M., Brücher, T., 2013. Were rivers flowing across the Sahara during the last interglacial? Implications for human migration through Africa. *PLoS One* 8 (9), e74834. <http://dx.doi.org/10.1371/journal.pone.0074834>.
- Croudace, I.W., Rindby, A., Rothwell, R.G., 2006. ITRAX: description and evaluation of a new multi-function X-ray core scanner. In: Rothwell, R.G. (Ed.), *New Techniques in Sediment Core Analysis*. Special Publication, vol. 267. Geological Society, London, pp. 51–63.
- Deino, A.L., Kingston, J.D., Glen, J.M., Edgar, R.K., Hill, A., 2006. Precessional forcing of lacustrine sedimentation in the late Cenozoic Chemeron Basin, Central Kenya Rift, and calibration of the Gauss/Matuyama boundary. *Earth Planet. Sci. Lett.* 247, 41–60.
- De Lange, G.J., Thomson, J., Reitz, A., Slomp, C.P., Speranza Principato, M., Erba, E., Corselli, C., 2008. Synchronous basin-wide formation and redox-controlled preservation of a Mediterranean sapropel. *Nat. Geosci.* 1, 606–610.
- deMenocal, P.B., 2004. African climate change and faunal evolution during the Pliocene-Pleistocene. *Earth Planet. Sci. Lett.* 220, 3–24.
- Deplazes, G., Lückge, A., Stuut, J.-B.W., Pätzold, J., Kuhlmann, H., Husson, D., Fant, M., Haug, G.H., 2014. Weakening and strengthening of the Indian monsoon during Heinrich events and Dansgaard-Oeschger oscillations. *Paleoceanography* 29, 99–114. <http://dx.doi.org/10.1002/2013PA002509>.
- Drake, N.A., Blench, R.M., Armitage, S.J., Bristow, C.S., White, K.H., 2010. Ancient water courses and biogeography of the Sahara explain the peopling of the desert. *Proc. Natl. Acad. Sci. U. S. A.* 108, 458–462. <http://dx.doi.org/10.1073/pnas.1012231108>.
- Drake, N.A., Breeze, P., Parker, A., 2013. Palaeoclimate in the Saharan and Arabian deserts during the middle Palaeolithic and the potential for hominin dispersals. *Quat. Int.* 300, 48–61.
- Ehrmann, W., Schmiedl, G., Beuscher, S., Krüger, S., 2017. Intensity of African humid periods estimated from Saharan dust fluxes. *PLoS One*. <http://dx.doi.org/10.1371/journal.pone.0170989>.
- Emeis, K.-C., Robertson, A.H.F., Richter, C., shipboard scientific party, 1996. Proceedings of the Ocean Drilling Program. Initial Reports, Leg 160. College Station, Texas.
- Emile-Geay, J., Tingley, M., 2016. Inferring climate variability from non-linear proxies: application to palaeo-ENSO studies. *Clim. Past* 12, 31–50.
- Feakins, S.J., 2013. Pollen-corrected leaf wax D/H reconstructions of northeast African hydrological changes during the late Miocene. *Palaeogeogr. Palaeoclimatol. Palaeoecol.* 374, 62–71.
- Feibel, C.S., 2011. A geological history of the Turkana Basin. *Evol. Anthropol.* 20, 206–216.
- Garcin, Y., Vincens, A., Williamson, D., Guiot, J., Buchet, G., 2006. Wet phases in tropical southern Africa during the last glacial period. *Geophys. Res. Lett.* 33, L07703. <http://dx.doi.org/10.1029/2005GL025531>.
- Gasse, F., 2000. Hydrological changes in the African tropics since the last glacial maximum. *Quat. Sci. Rev.* 19, 189–211.
- Geyh, M.A., Thiedig, F., 2008. The Middle Pleistocene Al Mahru'qah Formation in the Murzuq Basin, northern Sahara, Libya: evidence for orbitally-forced humid episodes during the last 500,000 years. *Palaeogeogr. Palaeoclimatol. Palaeoecol.* 257, 1–21.
- Govindaraju, K., 1994. A compilation of working values and descriptions for 383 geostandards. *Geostand. Newslett.* 18, 1–158.
- Grant, K.M., Grimm, R., Mikolajewicz, U., Ziegler, M., Rohling, E.J., 2016. The timing of Mediterranean sapropel deposition relative to insolation, sea-level and African monsoon changes. *Quat. Sci. Rev.* 140, 125–141. <http://dx.doi.org/10.1016/j.quascirev.2016.03.026>.
- Hennekam, R., De Lange, G., 2012. X-ray fluorescence core scanning of wet marine sediments: methods to improve quality and reproducibility of high resolution paleoenvironmental records. *Limnol. Oceanogr. Methods* 10, 991–1003. <http://dx.doi.org/10.4319/lom.2012.10.991>.
- Higgs, N.C., Thomson, J., Wilson, T.R.S., Croudace, I.W., 1994. Modification and complete removal of eastern Mediterranean sapropels by postdepositional oxidation. *Geology* 22, 423–426.
- Hilgen, F.J., 1991. Extension of the astronomically calibrated (polarity) to the Miocene/Pliocene boundary. *Earth Planet. Sci. Lett.* 107, 349–368.
- Jiang, N., Qiang, W., Leung, J.C.-H., 2016. The global monsoon division combining the k-means clustering method and low-level cross-equatorial flow. *Clim. Dyn.* 47, 2345–2359.
- Johnson, T.P., Werne, J.P., Brown, E.T., Abbott, A., Berke, M., Steinman, B.A., Halbur, J., Contreras, J., Grossheusch, S., Deino, A., Lyons, R.P., Scholz, C.A., Schouten, S., Sinnighe Damsté, J.S., 2016. A progressively wetter climate in southern East Africa over the past 1.3 million years. *Nature* 537, 220–224.
- Joordens, J.C.A., Vonhof, H.B., Feibel, C.S., Lourens, J.L., Dupont-Nivet, G., van der Lubbe, J.H.J.L., Sier, M.J., Davies, G.R., Kroon, D., 2011. An astronomically-tuned climate framework for hominins in the Turkana Basin. *Earth Planet. Sci. Lett.* 307, 1–18.
- Kageyama, M., Merkel, U., Otto-Bliesner, B., Prange, M., Abe-Ouchi, A., Lohmann, G., Ohgaito, R., Roche, D.M., Singarayer, J., Swingedouw, D., Zhang, X., 2013. Climatic impacts of fresh water hosing under Last Glacial Maximum conditions: a multi-model study. *Clim. Past* 9, 935–953.
- Kido, Y., Koshikawa, T., Tada, R., 2006. Rapid and quantitative major element analysis method for wet fine-grained sediments using an XRF microscanner. *Mar. Geol.* 229, 209–225. <http://dx.doi.org/10.1016/j.margeo.2006.03.002>.
- Kingston, J.D., Deino, A.L., Edgar, R.K., Hill, A., 2007. Astronomically forced climate change in the Kenyan rift valley 2.7–2.55 Ma: implications for the evolution of early hominin ecosystems. *J. Hum. Evol.* 53, 487–503.
- Konecky, B.L., Russell, J.M., Johnson, T.C., Brown, E.T., Berke, M.A., Werne, J.P., Huang, Y., 2011. Atmospheric circulation patterns during late Pleistocene climate changes at Lake Malawi, Africa. *Earth Planet. Sci. Lett.* 312, 318–326.
- Konijnenberg, T., Ziegler, M., Lourens, L., 2014. Chronological constraints on Pleistocene sapropel depositions from high-resolution geochemical records of ODP sites 967 and 968. *Newsletters Stratigr.* 47 (3), 263–282.
- Kuechler, R.R., Schefuß, E., Beckmann, B., Dupont, L., Wefer, G., 2013. NW African hydrology and vegetation during the Last Glacial cycle reflected in plant-wax-specific hydrogen and carbon isotopes. *Quat. Sci. Rev.* 82, 56–67.
- Kujau, A., Nürnberg, D., Zielhofer, C., Bahr, A., Röhle, U., 2010. Mississippi River discharge over the last ~56000 years—Indications from X-ray fluorescence core-scanning. *Palaeogeogr. Palaeoclimatol. Palaeoecol.* 298, 311–318. <http://dx.doi.org/10.1016/j.palaeo.2010.10.005>.
- Larrasoña, J.C., Roberts, A.P., Rohling, E.J., Winklhofer, M., Wehausen, R., 2003. Three million years of monsoon variability over the northern Sahara. *Clim. Dyn.* 21, 689–698.
- Larrasoña, J.C., Roberts, A.P., Rohling, E.J., 2013. Dynamics of green Sahara periods and their role in hominin evolution. *PLoS One* 8 (10), e76514. <http://dx.doi.org/10.1371/journal.pone.0076514>.
- Lebatard, A.E., Bourlès, D.L., Braucher, R., Arnold, M., Düringer, P., et al., 2010. Application of the authigenic $^{10}\text{Be}/^{9}\text{Be}$ dating method to continental sediments: reconstruction of the Mio-Pleistocene sedimentary sequence in the early hominin fossiliferous areas of the northern Chad Basin. *Earth Planet. Sci. Lett.* 297, 57–70.
- Lourens, L.J., 2004. Revised tuning of Ocean Drilling Program Site 964 and KC01B (Mediterranean) and implications for the d18O, tephra, calcareous nannofossil, and geomagnetic reversal chronologies of the past 1.1 Myr. *Paleoceanography* 19, PA3010.
- Lourens, L.J., Antonarakou, A., Hilgen, F.J., van Hoof, A.A.M., Vergnaud-Grazzini, C., Zachariasse, W.J., 1996. Evaluation of the Plio-Pleistocene astronomical timescale. *Paleoceanography* 11, 391–413.
- Lourens, L.J., Hilgen, F.J., Raffi, I., 1998. Base of large *Gephyrocapsa* and astronomical calibration of early Pleistocene sapropels in Site 967 and Hole 969D: solving the chronology of the Vrica section (Calabria, Italy). In: Robertson, A.H.F., Emeis, K.-C., Richter, C., Camerlenghi, A. (Eds.), *Proceedings of the Ocean Drilling Program, Scientific Results*, vol. 160. Ocean Drilling Program, College Station, TX, pp. 191–197.
- Lourens, L.J., Wehausen, R., Brumsack, H., 2001. Geological constraints on tidal dissipation and dynamical ellipticity of the earth over the past three million years. *Nature* 409, 1029–1033.
- Lourens, L.J., Hilgen, F.J., Shackleton, N.J., Laskar, J., Wilson, D., 2004. The Neogene period. In: Gradstein, F.M., Ogg, J.G., Smith, A.G. (Eds.), *A Geologic Timescale 2004*. Cambridge University Press, pp. 409–440.
- Lyons, R.P., Scholz, C.A., Cohen, A.S., King, J.W., Brown, E.T., Ivory, S.J., Johnson, T.C., Deino, A.L., Reinthal, P.N., McClung, M.M., Blome, M.W., 2015. Continuous 1.3-million-year record of East African hydroclimate, and implications for patterns of evolution and biodiversity. *PNAS*. <http://dx.doi.org/10.1073/pnas.1512864112>.
- MacLachlan, S.E., Hunt, J.E., Croudace, I.W., 2015. An empirical assessment of variable water content and grain size on X-ray fluorescence core-scanning measurements of deep sea sediments. In: Croudace, I.W., Rothwell, R.G. (Eds.), *Micro-xrf Studies of Sediment Cores*, vol. 17. Developments in paleoenvironmental research. <http://dx.doi.org/10.1007/978-94-017-9849-5-6>.
- Magill, C.R., Ashley, G.M., Freeman, K., 2013. Ecosystem variability and early human habitats in eastern Afr. *Afr. Proc. Natl. Acad. Sci.* 110, 1167–1174.
- Maslin, M.A., Brierley, C.M., Milner, A.M., Shultz, S., Trauth, M.H., Wilson, K.E., 2014. East African climate pulses and early human evolution. *Quat. Sci. Rev.* 101, 1–17.
- Mulitza, S., Prange, M., Stuut, J., Zabel, M., von Dobeneck, T., Itambi, A.C., Nizou, J., Schulz, M., Wefer, G., 2008. Sahel megadroughts triggered by glacial slowdowns of Atlantic meridional overturning. *Paleoceanography* 23, PA4206. <http://dx.doi.org/10.1029/2008PA001637>.
- Nicholson, S.E., 1996. A review of climate dynamics and climate variability in Eastern Africa. In: Johnson, T.C., Odada, E.O. (Eds.), *The Limnology, Climatology and Paleoclimatology of the East African Lakes*. Gordon and Breach, Amsterdam,

- pp. 25–56.
- Nicholson, S., 2000. The nature of rainfall variability over Africa on time scales of decades to millenia. *Glob. Planet. Change* 26, 137–158.
- Nicholson, S.E., 2009. A revised picture of the structure of the “monsoon” and land ITCZ over West Africa. *Clim. Dyn.* 32, 1155–1171.
- Niedermeyer, E.M., Schefuß, E., Sessions, A.L., Mulitza, S., Mollenhauer, G., Schulz, M., Wefer, G., 2010. Orbital- and millennial-scale changes in the hydrologic cycle and vegetation in the western African Sahel: insights from individual plant wax δD and δ¹³C. *Quat. Sci. Rev.* 29, 2996–3005.
- Nijenhuis, I.A., Bosch, H.J., Sinnighe Damsté, J.S., Brumsack, H.-J., de Lange, G.J., 1999. Organic matter and trace element rich sapropels and black shales: a geochemical comparison. *Earth Planet. Sci. Lett.* 169, 277–290.
- Osborne, A.H., Vance, D., Rohling, E.J., Barton, N., Rogerson, M., Fello, N., 2008. A humid corridor across the Sahara for the migration “Out of Africa” of early modern humans 120,000 years ago. *Proc. Natl. Acad. Sci. U. S. A.* 105, 16444–16447.
- Otto-Btiesner, B., Russell, J.M., Clark, P.U., Liu, Z., Overpeck, J.T., Konecky, B., deMenocal, P., Nicholson, S.E., He, F., Lu, Z., 2014. Coherent changes of southeastern equatorial and northern African rainfall during the last deglaciation. *Science* 346, 1223–1227.
- Paillou, P., Schuster, M., Tooth, S., Farr, T., Rosenqvist, A., Lopez, S., Malezieux, J.M., 2009. Mapping of a major paleodrainage system in eastern Libya using orbital imaging radar: the Kufrah River. *Earth Planet. Sci. Lett.* 277, 327–333.
- Passier, H.F., De Lange, G.F., 1998. Sedimentary sulfur and iron chemistry in relation to the formation of eastern Mediterranean sapropels. In: Robertson, A.H.F., Emeis, K.C., Richter, C., Camerlenghi, A. (Eds.), *Proc. ODP, Sci. Results*, vol. 160, pp. 249–259.
- Petit-Maire, N., Casta, L., Delibrias, G., Gaven, Ch., with appendix by Testud, A.-M., 1980. In: Salem, M.J., Busrewil, M.T. (Eds.), *Preliminary Data on Quaternary Palaeolacustrine Deposits in the Wadi Ash Shati Area, Libya. The Geology of Libya III*. Academic Press, London, pp. 797–807.
- Revel, M., Ducassou, E., Groussset, F.E., Bernasconi, S.M., Migeon, S., Revillon, S., Mascle, J., Murat, A., Zaragosi, S., Bosch, D., 2010. 100,000 years of African monsoon variability recorded in sediments of the Nile margin. *Quat. Sci. Rev.* 29, 1342–1362.
- Ritchie, J.C., Eyles, C.H., Haynes, C.V., 1985. Sediment and pollen evidence for an early to mid-Holocene humid period in the eastern sahara. *Nature* 314, 352–355.
- Rohling, E.J., Bryden, H.L., 1994. Estimating past changes in the eastern Mediterranean freshwater budget, using reconstructions of sea level and hydrography. *Proc. K. Ned. Akad. Wet. Ser. B* 97, 201–217.
- Rohling, E.J., Cane, T.R., Cooke, S., Sprovieri, M., Bouloubassi, I., Emeis, K.C., Schiebel, R., Kroon, D., Jorissen, F.J., Lorre, A., Kemp, A.E.S., 2002. African monsoon variability during the previous interglacial maximum. *Earth Planet. Sci. Lett.* 202, 61–75.
- Rohling, E.J., Sprovieri, M., Cane, T.R., Casford, J.S.L., Cooke, S., Bouloubassi, I., Emeis, K.C., Schiebel, R., Hayes, A., Jorissen, F.J., Kroon, D., 2004. Reconstructing past planktonic foraminiferal habitats using stable isotope data: a case history for Mediterranean sapropel S5. *Mar. Micropaleontol.* 50, 89–123.
- Rohling, E.J., Grant, K.M., Marino, G., Roberts, A.P., Larrasoña, J.C., 2013. Paleoclimate variability in the Mediterranean and red sea regions during the last 500,000 Years. *Curr. Anthropol.* 54 (8). <http://www.jstor.org/stable/10.1086/673882>.
- Rohling, E.J., Foster, G.L., Grant, K.M., Marino, G., Roberts, A.P., Tamisiea, M.E., Williams, F., 2014. Sea-level and deep-sea-temperature variability over the past 5.3 million years. *Nature* 508, 477–482.
- Rohling, E.J., Marino, G., Grant, K., 2015. Mediterranean climate and oceanography, and the periodic development of anoxic events (sapropels). *Earth-Sci. Rev.* 143, 62–97.
- Rose, C., Polissar, P.J., Tierney, J.E., Filley, T., deMenocal, P.B., 2016. Changes in northeast African hydrology and vegetation associated with Pliocene–Pleistocene sapropel cycles. *Phil. Trans. R. Soc. B* 371, 20150243. <http://dx.doi.org/10.1098/rstb.2015.0243>.
- Rossignol-Strick, M., 1985. Mediterranean quaternary sapropels, an immediate response of the African monsoon to variation of insolation. *Palaeogeography, Palaeoclimatology, Palaeoecology* 49, 237–263.
- Rossignol-Strick, M., Nesteroff, W., Olive, P., Vergnaud-Grazzini, C., 1982. After the deluge: Mediterranean stagnation and sapropel formation. *Nature* 295, 105–110.
- Rothwell, R.G., Croudace, I.W., 2015. Micro-XRF studies of sediment cores: a perspective on capability and application in the environmental sciences. In: Croudace, I.W., Rothwell, R.G. (Eds.), *Micro-xrf Studies of Sediment Cores*, vol. 17. Developments in paleoenvironmental research. <http://dx.doi.org/10.1007/978-94-017-9849-5-1>.
- Rousseeuw, P.J., van Zomeren, B.C., 1990. Unmasking multivariate outliers and leverage points. *J. Am. Stat. Assoc.* 85, 633–639.
- Sakamoto, T., Janecek, T., Emeis, K.-C., 1998. Continuous sedimentary sequences from the eastern Mediterranean sea: composite depth sections. In: Robertson, A.H.F., Emeis, K.-C., Richter, C., Camerlenghi, A. (Eds.), *Proceedings of the Ocean Drilling Program, Scientific Results*, vol. 160. Ocean Drilling Program, College Station, TX, pp. 37–60.
- Santer, B.D., Wigley, T.M.L., Boyle, J.S., Gaffen, D.J., Hnilo, J.J., Nychka, D., Parker, D.E., Taylor, K.E., 2000. Statistical significance of trends and trend differences in layer-average atmospheric temperature time series. *J. Geophys. Res.* 105, 7337–7356.
- Satow, C., 2012. The Tephrostratigraphy of Three, Late Quaternary, Mediterranean Marine Cores. PhD Thesis. University of London, Royal Holloway.
- Schneider, T., Bischoff, T., Haug, G.H., 2014. Migrations and dynamics of the inter-tropical convergence zone. *Nature* 513, 45–53.
- Shanahan, T.M., McKay, N.P., Hughen, K.A., Overpeck, J.T., Otto-Bliesner, B., Heil, C.W., King, J., Scholz, C.A., Peck, J., 2015. The time-transgressive termination of the African humid period. *Nat. Geosci.* 8 <http://dx.doi.org/10.1038/NGEO2329>.
- Singarayer, J.S., Burrough, S.L., 2015. Interhemispheric dynamics of the African rainbelt during the late Quaternary. *Quat. Sci. Rev.* 124, 48–67.
- Skonieczny, C., Paillou, P., Bory, A., Bayon, G., Biscara, L., Crosta, X., Eynaud, F., Malaiéz, B., Revel, M., Aleman, N., Barusseau, J.-P., Vernet, R., Lopez, S., Groussset, F., 2015. African humid periods triggered the reactivation of a large river system in Western Sahara. *Nat. Commun.* 6, 8751. <http://dx.doi.org/10.1038/ncomms9751>.
- Street, F.A., Grove, A.T., 1976. Environmental and climatic implications of late Quaternary lake-level fluctuations in Africa. *Nature* 261, 385–390.
- Szabo, B.J., Haynes Jr., C.V., Maxwell, T.A., 1995. Ages of Quaternary pluvial episodes determined by uranium-series and radiocarbon dating of lacustrine deposits of Eastern Sahara. *Palaeogeogr. Palaeoclimatol. Palaeoecol.* 113, 227–242.
- Thomson, J., Mercone, D., de Lange, G.J., van Santvoort, P.J.M., 1999. Review of recent advances in the interpretation of eastern Mediterranean sapropel S1 from geochemical evidence. *Mar. Geol.* 153, 77–89.
- Tiedemann, R., Sarnthein, M., Shackleton, N.J., 1994. Astronomic timescale for the Pliocene Atlantic 180° and dust flux records of ocean drilling Program site 659. *Paleoceanography* 9, 619–638.
- Tierney, J.E., deMenocal, P.B., 2013. Abrupt shifts in Horn of Africa hydroclimate since the Last Glacial Maximum. *Science* 342, 843–846.
- Tierney, J.E., Russell, J.M., Huang, Y., Damsté, J.S.S., Hopmans, E.C., Cohen, A.S., 2008. Northern hemisphere controls on tropical southeast African climate during the past 60,000 years. *Science* 322, 252–255.
- Tierney, J.E., Lewis, S.C., Cook, B.I., LeGrande, A.N., Schmidt, G.A., 2011. Model, proxy and isotopic perspectives on the East African humid period. *Earth Planet. Sci. Lett.* 307, 103–112.
- Timmermann, A., Friedrich, T., 2016. Late Pleistocene climate drivers of early human migration. *Nature* 538, 92–95. <http://dx.doi.org/10.1038/nature19365>.
- Tjallingii, R., Röhl, U., Kölling, M., Bickert, T., 2007. Influence of the water content on X-ray fluorescence core-scanning measurements in soft marine sediments. *Geochem., Geophys., Geosyst.* 8 <http://dx.doi.org/10.1029/2006GC001393>.
- Tjallingii, R., Claussen, M., Stuut, J.-B.W., Fohlmeister, J., Jahn, A., Bickert, T., Lamy, F., Röhl, U., 2008. Coherent high- and low-latitude control of the northwest African can hydrological balance. *Nat. Geosci.* 1, 670–675.
- Trauth, M.H., Larrasoña, J.C., Mudelsee, M., 2009. Trends, rhythms and events in Plio-Pleistocene African climate. *Quat. Sci. Rev.* 28, 399–411.
- Trauth, M.H., Maslin, M.A., Deino, A., Strecker, M.R., 2005. Late Cenozoic moisture history of East Africa. *Science* 309, 2051–2053.
- Van Os, B.J.H., Middelburg, J.J., De Lange, G.J., 1991. Possible diagenetic mobilisation of barium in sapropelic sediment from the eastern Mediterranean. *Mar. Geol.* 100, 125–136.
- Van Os, B.J.H., Lourens, L.J., Hilgen, F.J., De Lange, G.J., 1994. The Formation of Pliocene sapropels and carbonate cycles in the Mediterranean: Diagenesis, dilution, and productivity. *Paleoceanography* 9, 601–617.
- Van Santvoort, P.J.M., de Lange, G.J., Langereis, C.G., Dekkers, M.J., Paterne, M., 1997. Geochemical and paleomagnetic evidence for the occurrence of “missing” sapropels in eastern Mediterranean sediments. *Paleoceanography* 12, 773–786.
- Voelker, A.H.L., 2002. Global distribution of centennial-scale records for marine isotope stage (MIS) 3: a database. *Quat. Sci. Rev.* 21 (10), 1185–1212. [http://dx.doi.org/10.1016/S0277-3791\(01\)00139-1](http://dx.doi.org/10.1016/S0277-3791(01)00139-1).
- Wang, P.X., Wang, B., Cheng, H., Fusillo, J., Guo, Z.T., Kiefer, T., Liu, Z.Y., 2014. The global monsoon across timescales: coherent variability of regional monsoons. *Clim. Past.* 10, 2007–2052.
- Wang, Y.J., Cheng, H., Edwards, R.L., An, Z.S., Wu, J.Y., Shen, C.C., Dorale, J.A., 2001. A high-resolution absolute-dated late Pleistocene monsoon record from Hulu Cave, China. *Science* 294, 2345–2348.
- Wehausen, R., Brumsack, H.J., 2000. Chemical cycles in Pliocene sapropel-bearing and sapropel-barren eastern Mediterranean sediments. *Palaeogeogr. Palaeoclimatol. Palaeoecol.* 158, 325–352.
- Weldeab, S., Lea, D.W., Schneider, R.R., Andersen, N., 2007. 155,000 years of West African monsoon and ocean thermal evolution. *Science* 316, 1303–1307.
- Weltje, G.J., Tjallingii, R., 2008. Calibration of XRF core scanners for quantitative geochemical logging of sediment cores: Theory and application. *Earth Plan. Sci. Lett.* 274, 423–438.
- Weltje, G.J., Bloemsma, M.R., Tjallingii, R., Heslop, D., Röhl, U., 2015. Prediction of geochemical composition from XRF core scanner data: a new multivariate approach including automatic selection of calibration samples and quantification of uncertainties. In: Croudace, I.W., Rothwell, R.G. (Eds.), *Micro-xrf Studies of Sediment Cores*, vol. 17. Developments in paleoenvironmental research. <http://dx.doi.org/10.1007/978-94-017-9849-5-21>.
- Wien, K., Holz, C., Kölling, M., Schulz, H.D., 2006. Age models for pelagites and turbidites from the Cap timiris canyon off Mauritania. *Mar. Petroleum Geol.* 23, 337–352.
- Winkler, G., Anderson, R.F., Fleischer, M.Q., McGee, D., Mahowald, N., 2008. Covariant glacial-interglacial dust fluxes in the equatorial Pacific and Antarctica. *Science* 320, 93–96.
- Woodward, J.C., 2009. The Physical Geography of the Mediterranean. Oxford University Press, Oxford. ISBN: 978-0-19-926803-0.

- Zabel, M., Bickert, T., Dittert, L., Haese, R.R., 1999. The significance of the sedimentary Al/Ti ratio as indicator for reconstructions of the terrestrial input to the equatorial Atlantic. *Paleoceanography* 14, 789–799.
- Zabel, M., Schneider, R.R., Wagner, T., Adegbie, A.T., de Vries, U., Kolonic, S., 2001. Late quaternary climate changes in central Africa as inferred from terrigenous input to the Niger fan. *Quat. Res.* 56, 207–217.
- Zhao, Y., 2011. Variations of the Nile suspended discharges during the last 1.75 Myr. *Palaeogeography, Palaeoclimatology, Palaeoecology* 311, 230–241.
- Ziegler, M., Tuenter, E., Lourens, L.J., 2010. The precession phase of the boreal summer monsoon as viewed from the eastern Mediterranean (ODP Site 968). *Quat. Sci. Rev.* 29, 1481–1490.